IOP Publishing Journal of Physics: Condensed Matter
J. Phys.: Condens. Matter **26** (2014) 493203 (20pp) doi:10.1088/0953-8984/26/49/493203

Topical Review

Unconventional symmetries of Fermi liquid and Cooper pairing properties with electric and magnetic dipolar fermions

Yi Li[1] **and Congjun Wu**[2]

[1] Princeton Center for Theoretical Science, Princeton University, Princeton, NJ 08544, USA
[2] Department of Physics, University of California, San Diego, CA 92093, USA

E-mail: wucj@physics.ucsd.edu

Received 2 September 2014
Accepted for publication 30 September 2014
Published 17 November 2014

Abstract

The rapid experimental progress of ultra-cold dipolar fermions opens up a whole new opportunity to investigate novel many-body physics of fermions. In this article, we review theoretical studies of the Fermi liquid theory and Cooper pairing instabilities of both electric and magnetic dipolar fermionic systems from the perspective of unconventional symmetries. When the electric dipole moments are aligned by the external electric field, their interactions exhibit the explicit $d_{r^2-3z^2}$ anisotropy. The Fermi liquid properties, including the single-particle spectra, thermodynamic susceptibilities and collective excitations, are all affected by this anisotropy. The electric dipolar interaction provides a mechanism for the unconventional spin triplet Cooper pairing, which is different from the usual spin-fluctuation mechanism in solids and the superfluid ^{3}He. Furthermore, the competition between pairing instabilities in the singlet and triplet channels gives rise to a novel time-reversal symmetry breaking superfluid state. Unlike electric dipole moments which are induced by electric fields and unquantized, magnetic dipole moments are intrinsic proportional to the hyperfine-spin operators with a Lande factor. Its effects even manifest in unpolarized systems exhibiting an isotropic but spin–orbit coupled nature. The resultant spin–orbit coupled Fermi liquid theory supports a collective sound mode exhibiting a topologically non-trivial spin distribution over the Fermi surface. It also leads to a novel p-wave spin triplet Cooper pairing state whose spin and orbital angular momentum are entangled to the total angular momentum $J = 1$ dubbed the J-triplet pairing. This J-triplet pairing phase is different from both the spin–orbit coupled ^{3}He-B phase with $J = 0$ and the spin–orbit decoupled ^{3}He-A phase.

Keywords: electric and magnetic dipolar interactions, anisotropic Fermi liquid theory, spin–orbit coupled Fermi liquid theory, p-wave triplet Cooper pairing, time-reversal symmetry breaking

(Some figures may appear in colour only in the online journal)

1. Introduction

Dipolar interactions have become a major research focus of ultra-cold atomic and molecular physics. For bosonic atoms with large magnetic dipolar moments (e.g. ^{52}Cr), their magnetic moments are aligned in the Bose–Einstein condensates in which the anisotropy of the dipolar interaction is manifested [1–7]. On the other hand, the synthesis and cooling of both fermions with electric and magnetic dipolar moments give rises to an even more exciting opportunity to explore novel many-body physics [8–26]. The quantum degeneracy of the fermionic dipolar molecules of ^{40}K^{87}Rb has

been realized [8–10]. These molecules have been loaded into optical lattices in which the loss rate is significantly suppressed [11, 15]. The chemically stable dipolar molecules of $^{23}Na^{40}K$ have been cooled down to nearly quantum degeneracy with a lifetime reported as 100 ms near the Feshbach resonance [12]. The quantum degeneracy of fermionic atoms with large magnetic dipole moments has also been achieved for the systems of ^{161}Dy with $10\,\mu_B$ [21, 26, 27] and ^{167}Er with $7\,\mu_B$ [18–20], which are characterized by the magnetic dipolar interaction.

Electric and magnetic dipolar fermions exhibit novel many-body physics that is not well-studied in usual solids. One of the most prominent features of the electric dipolar interaction is spatial anisotropy, which is markedly different from the isotropic Coulomb interaction in solids. In contrast, the magnetic dipolar interaction remains isotropic in unpolarized systems. More importantly, it exhibits the spin–orbit (SO) coupled feature, i.e. the magnetic dipolar interaction is invariant only under the simultaneous rotation of both the orientations of magnetic moments and their relative displacement vectors. These features bring interesting consequences to the many-body physics of dipolar fermions.

Rigorously speaking, so far there are still no permanent electric dipole moments having been discovered yet at the levels of the elementary particle, atom and molecule. For example, for a hetero-nuclear dipolar molecule, even though at an instantaneous moment, it exhibits a dipole moment, while it averages to zero in the molecular rotational eigenstates. External electric fields are needed to polarize electric dipole moments, which mixes rotational eigenstates with opposite parities. However, the dipole moment of these mixed states is unquantized and, thus the electric dipole moment is a classic vector. When two dipole moments are aligned, say, along the z-axis, the interaction between them is spatially anisotropic, which not only depends on the distance between two dipoles, but also the direction of the relative displacement vector. Nevertheless, this anisotropy exhibits an elegant form of the spherical harmonics of the second Legendre polynomial, i.e. the $d_{r^2-3z^2}$-type anisotropy [28–30]. This elegant anisotropy greatly simplifies the theoretical study of the novel many-body physics with the electric dipolar interaction.

The electric dipolar interaction results in an anisotropic Fermi liquid state, which exhibits different single-particle and collective properties from those of the standard isotropic Fermi liquid theory [31–42]. The shape of the Fermi surface exhibits anisotropic distortions [31, 32, 34, 40, 43]. The anisotropic dipolar interaction mixes different partial-wave channels and thus the usual Landau interaction parameters in the isotropic case should be generalized into the Landau interaction matrix with a tri-diagonal structure, which renormalizes thermodynamic susceptibilities [33, 34]. The dispersion of the collective zero sound mode is also anisotropic: the zero sound mode can only propagate in a certain range of the solid angle direction and its sound velocity is maximal if the propagation direction is along the north or south poles [34, 36].

The anisotropy of the electric dipolar interaction also results in unconventional Cooper pairing symmetries [28, 29, 44–54]. The electric dipolar interaction is neither purely attractive nor purely repulsive. The partial-wave analysis shows that the most attractive pairing channel is p_z-like, which naturally gives rise to a new mechanism to unconventional pairing symmetry. Consequently, for the single component case, the pairing symmetry is mostly of p_z-like slightly hybridized with even higher odd partial wave components [28, 29, 44, 45]. The pairing structure of the two-component dipolar fermions is even more interesting, which allows both the $s + d$-wave channel singlet and the p_z-wave triplet pairings [50, 52, 53, 55]. The dipolar interaction induced triplet pairing is to first order in interaction strength. In comparison, the spin fluctuation mechanism in solid state systems (e.g. ^3He and Sr_2RuO_4) is a higher order effect of interactions [56, 57]. The singlet and triplet pairing symmetries can coexist in two-component electric dipolar fermion systems. Only when their relative phase angle is $\pm\frac{\pi}{2}$, the resultant pairing is unitary [50]. This gives rise to a novel and very general mechanism to a spontaneous time-reversal (TR) symmetry breaking pairing state.

Next we discuss the novel feature of the magnetic dipolar fermions [43, 58–65]. The magnetic dipolar interaction is very complicated to handle in classic systems, which leads to a variety of rich patterns in real space. In comparison, for the quantum degenerate Fermi systems, the existence of Fermi surfaces constraints the low energy degrees of freedom only around the Fermi surface. This feature greatly simplifies the theoretical analysis and the exotic physics with non-trivial spin texture patterns lies in momentum space instead of real space.

Typically speaking, the interaction energy scale of magnetic dipolar fermions is much smaller than that of the electric dipolar case. Nevertheless, conceptually they are still very interesting. Unlike the electric dipolar moment, the magnetic moment is proportional to the hyperfine-spin with the Lande factor and thus its components are non-commutative quantum-mechanical operators [60, 62]. Magnetic dipole moments are permanent in the sense that they do not need to be induced by external magnetic fields. In the absence of external fields, the unpolarized magnetic dipolar systems are in fact isotropic. Neither spin nor orbital angular momentum is conserved; nevertheless, the total angular momentum remains conserved by the dipolar interaction. Thus the magnetic dipolar interaction exhibits the essential feature of the SO coupling physics. Very recently, using electric dipolar moments to generate effective SO coupled interactions similar to that in the magnetic dipolar systems is also proposed in [17] by properly coupling microwaves to molecular rotation eigenstates.

The ordinary SO coupling in solids is a single-particle effect originating from the relativistic physics. In contrast, in magnetic dipolar fermion systems [59, 61, 62], the Fermi surfaces remain spherical without splitting in the absence of the external magnetic fields. Nevertheless, this SO coupling appears at the interaction level, including the SO coupled Fermi surface Pomeranchuk instabilities [59, 61, 62] and topological zero-sound wave modes exhibiting an oscillating spin distribution of the hedgehog-type configuration over the Fermi surface [62].

The magnetic dipolar interaction also induces novel Cooper pairing structures exhibiting the SO coupled nature

[60, 66]. Even in the simplest case of $F = \frac{1}{2}$, the magnetic dipolar interaction provides a novel and robust mechanism for the p-wave ($L = 1$) spin triplet ($S = 1$) Cooper pairing which arises from the attractive channel of the magnetic dipolar interaction. It turns out that its pairing symmetry structure is markedly different from that in the celebrated p-wave pairing system of ^{3}He: the orbital angular momenta L and spin S of Cooper pairs are entangled into the channel of the total angular momentum $J = 1$, dubbed as the J-triplet pairing. In comparison, the ^{3}He-B phase is isotropic in which $J = 0$, while the A-phase is anisotropic in which J is not well-defined [56].

In this article, we review the recent progress of the novel many-body physics with dipolar fermions, such as the Fermi liquid properties and Cooper pairing structures, focusing on unconventional symmetries. In section 2, we review the anisotropy of the electric dipolar interaction and the SO structure of the magnetic dipolar interactions, respectively, from the viewpoint of their Fourier components. In section 3, the anisotropic Fermi liquid theory of the electric dipolar fermions is reviewed. And the SO coupled Fermi liquid theory of the magnetic dipolar fermion systems is reviewed in section 4. The p_z-wave Cooper pairing in the single and two-component electric dipolar systems and the TR reversal symmetry breaking effect are reviewed in section 5. The SO coupled Cooper pairing with the J-triplet structure in the magnetic dipolar fermion systems is reviewed in section 6. Conclusions and outlooks are presented in section 7.

Due to limit of space and also the view point from the unconventional symmetry, we are not able to cover many important research directions of dipolar atoms and molecules in this review. For example, the progress on topics of strong correlation physics with dipolar fermions [67–69], the Feshbach resonance with dipolar fermions [52, 53], the synthetic gauge field with dipolar fermions [70, 71] and the engineering of exotic and topological many-body states [72–74]. Some of these progresses have been excellently reviewed in [17, 30]. The properties of dipolar boson condensations are not covered here either and there are already many important reviews on this topic [1, 3, 3, 30, 75, 76].

2. Fourier transform of dipolar interactions

In this section, we review the Fourier transformations of both the electric and magnetic dipolar interactions in section 2.1 and section 2.2, respectively. The anisotropy of the electric dipolar interaction and the SO coupled feature of the magnetic dipolar interaction also manifest in their momentum space structure. These Fourier transforms are important for later analysis of many-body physics.

2.1. Electric dipolar interaction

Without loss of generality, we assume that all the electric dipoles are aligned by the external electric field $\vec{E}$ along the z-direction, then the dipolar interaction between two dipole moments is [28, 29]

$$V_d(\vec{r}_{12}) = -\frac{2d^2}{|r_{12}|^3} P_2(\cos\theta_{12}), \tag{1}$$

where d is the magnitude of the electric dipole moment; $\vec{r}_{12} = \vec{r}_1 - \vec{r}_2$ is the displacement vector between two dipoles; θ_{12} is the polar angle of $\vec{r}_{12}$; $P_2(\cos\theta_{12})$ is the standard second Legendre polynomial as

$$P_2(\cos\theta_{12}) = \frac{1}{2}(3\cos^2\theta_{12} - 1).$$

The zeros of the second Legendre polynomial lie around the latitudes of θ_0 and $\pi - \theta_0$ with

$$\theta_0 = \cos^{-1}\frac{1}{\sqrt{3}} \approx 55^\circ. \tag{2}$$

Within $\theta_0 < \theta_{12} < \pi - \theta_0$, the dipolar interaction is repulsive and otherwise, it is attractive. The spatial average of the dipolar interaction in 3D is zero.

For later convenience, we introduce the Fourier transform of the dipolar interaction equation (1),

$$V_d(\vec{q}) = \int \mathrm{d}^3\vec{r}\, \mathrm{e}^{-\mathrm{i}\vec{q}\cdot\vec{r}} V_d(\vec{r}). \tag{3}$$

A lot of information can be obtained solely based on symmetry and dimensional analysis. First, $\mathrm{e}^{\mathrm{i}\vec{q}\cdot\vec{r}}$ is invariant under spatial rotations, thus $V_d(\vec{q})$ transforms the same as $V_d(\vec{r})$ under spatial rotations. It should exhibit the same symmetry factor of the spherical harmonics. Second, since $V_d(\vec{r})$ decays with a cubic law, $V_d(\vec{q})$ should be dimensionless.

If $V_d(\vec{r}_{12})$ were isotropic, $V_d(\vec{q})$ would logarithmically depends on q. However, a more detailed calculation shows that actually it does not depend on the magnitude of q. Let us introduce a short distance cutoff ϵ that the dipolar interaction equation (1) is only valid for $r \geqslant \epsilon$ and a long distance cutoff R as the radius of the system. A detailed calculation shows that [34]

$$V_d(\vec{q}) = 8\pi d^2 \left\{ \frac{j_1(q\epsilon)}{q\epsilon} - \frac{j_1(qR)}{qR} \right\} P_2(\cos\theta_{\vec{q}}) \tag{4}$$

where $j_1(x)$ is the first order spherical Bessel function with the asymptotic behavior as

$$j_1(x) \to \begin{cases} \dfrac{x}{3}, & \text{as} \quad x \to 0; \\ \dfrac{1}{x}\sin\left(x - \dfrac{\pi}{2}\right), & \text{as} \quad x \to \infty. \end{cases} \tag{5}$$

After taking the limits of $q\epsilon \to 0$ and $qR \to +\infty$, we arrive at

$$V_d(\vec{q}) = \frac{8\pi d^2}{3} P_2(\cos\theta_{\vec{q}}). \tag{6}$$

At $\vec{q} = 0$, $V_d(\vec{q} = 0)$ is defined as 0 based on the fact that the angular average of the 3D dipolar interaction vanishes, thus V_d is singular as $\vec{q} \to 0$. Even in the case that R is large but finite, the smallest nonzero value of qR is at the order of $O(1)$. Thus, $V_d(\vec{q})$ remains non-analytic as $\vec{q} \to 0$.

An interesting feature of the above Fourier transform equation (6) is that the anisotropy in momentum space is opposite to that in real space: it is most negative when $\vec{q}$ lies in the equatorial plane and most positive when $\vec{q}$ points to the

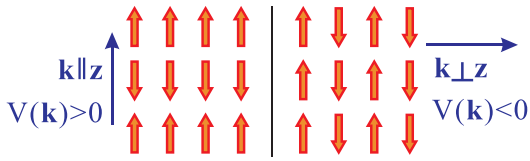

Figure 1. The Fourier components of the dipolar interaction $V_d(\vec{k})$. The left-hand-side is for $\vec{k} \parallel \hat{z}$ and the right-hand-side is for $\vec{k} \perp \hat{z}$.

north and south poles. An intuitive picture is explained in figure 1. Consider a spatial distribution of the dipole density $\rho(r)$, then the classic interaction energy is

$$\int\int \mathrm{d}r_1 \mathrm{d}r_2 \rho(\vec{r}_1)\rho(\vec{r}_2)V_d(\vec{r}_1-\vec{r}_2) = \frac{1}{V_0}\sum_{\vec{q}}|\rho(\vec{q})|^2 \times V_d(\vec{q}), \tag{7}$$

where V_0 is the system volume. If the wave vector $\vec{q}$ is along the z-axis, then the dipole density oscillates along the dipole orientation, thus the interaction energy is repulsive. On the other hand, if $\vec{q}$ lies in the equatorial plane, the dipole density oscillates perpendicular to the dipole orientation and thus the interaction energy is attractive.

2.2. Magnetic dipolar interaction

Now let us consider the magnetic dipolar interaction [18–21, 26, 27]. Different from the electric dipole moment, the magnetic one originates from contributions of several different angular momentum operators. The total magnetic moment is not conserved and thus its component perpendicular to the total spin averages to zero. For the low energy physics below the coupling energy among different angular momenta, the magnetic moment can be approximated as just the component parallel to the spin direction and thus the effective magnetic moment is proportional to the hyperfine spin operator up to a Lande factor and thus is a quantum mechanical operator. Due to the large difference of energy scales between the fine and hyperfine structure couplings, the effective atomic magnetic moment below the hyperfine energy scale can be calculated through the following two steps. The first step is the Lande factor for the electron magnetic moment respect to total angular momentum of electron defined as $\vec{\mu}_e = g_J\mu_B\vec{J}$, where μ_B is the Bohr magneton; $\vec{J} = \vec{L} + \vec{S}$ is the sum of electron orbital angular momentum $\vec{L}$ and spin $\vec{S}$; and the value of g_J is determined as

$$g_J = \frac{g_L+g_s}{2} + \frac{g_L-g_s}{2}\frac{L(L+1)-S(S+1)}{J(J+1)}. \tag{8}$$

Further considering the hyperfine coupling, the total magnetic momentum is defined $\vec{\mu} = \mu_B(g_J\vec{J} + g_I\vec{I}) = g_F\vec{F}$ where g_I is proportional to the nuclear gyromagnetic ratio and is thus tiny and $\vec{F}$ is the hyperfine spin. The Lande factor g_F can be similarly calculated as

$$g_F = \frac{g_J+g_I}{2} + \frac{g_J-g_I}{2}\frac{J(J+1)-I(I+1)}{F(F+1)} \approx \frac{g_J}{2}\left(1+\frac{J(J+1)-I(I+1)}{F(F+1)}\right). \tag{9}$$

The magnetic dipolar interaction between two spin-F atoms located at $\vec{r}_1$ and $\vec{r}_2$ is

$$V_{\alpha\beta;\beta'\alpha'}(\vec{r}) = \frac{g_F^2\mu_B^2}{r^3}\left[\vec{F}_{\alpha\alpha'}\cdot\vec{F}_{\beta\beta'} - 3(\vec{F}_{\alpha\alpha'}\cdot\hat{r})(\vec{F}_{\beta\beta'}\cdot\hat{r})\right], \tag{10}$$

where $\vec{r} = \vec{r}_1 - \vec{r}_2$ and $\hat{r} = \vec{r}/r$ is the unit vector along $\vec{r}$. Similarly to the case of the electric dipolar interaction, the Fourier transform of equation (10) possesses the same symmetry structure as that in real space [43, 59]

$$V_{\alpha\beta;\beta'\alpha'}(\vec{q}) = \frac{4\pi g_F^2\mu_B^2}{3}\left[3(\vec{F}_{\alpha\alpha'}\cdot\hat{q})(\vec{F}_{\beta\beta'}\cdot\hat{q}) - \vec{F}_{\alpha\alpha'}\cdot\vec{F}_{\beta\beta'}\right]. \tag{11}$$

Again, it only depends on the direction of the momentum transfer but not on its magnitude and it is also singular as $\vec{q}\to 0$. If $\vec{q}$ is exactly zero, $V_{\alpha\beta;\beta'\alpha'}(\vec{q}=0) = 0$.

In the current experiment systems of magnetic dipolar atoms, the atomic spin is very large. For example, for ^{161}Dy, its atomic spin reaches $F = \frac{21}{2}$ and thus an accurate theoretical description of many-body physics of the magnetic dipolar interactions of such a large spin system would be quite challenging [21, 26]. Nevertheless, as a theoretical starting point, we can use the case of $F = \frac{1}{2}$ as a prototype model which exhibits nearly all the qualitative features of the magnetic dipolar interactions [43, 60].

3. Anisotropic Fermi liquid theory of electric dipolar fermions

In this section, we will review the new ingredients of the Fermi liquid theory brought by the anisotropic electric dipolar interaction [31–39, 41, 42], including the single-particle properties such as Fermi surface distortions and two-body properties including thermodynamic properties and collective modes.

A general overview of the Landau–Fermi liquid theory is presented in section 3.1. In section 3.2, we review the dipolar interaction induced Fermi surface distortions. The Landau interaction matrix is presented in section 3.3 and its renormalization on thermodynamic properties including Pomeranchuk instabilities are review in section 3.4. The anisotropic collective excitations are reviewed in section 3.5.

3.1. A quick overview of the Fermi liquid theory

One of the most important paradigms of the interacting fermion systems is the Landau Fermi liquid theory [77–79]. The Fermi liquid ground state can be viewed as an adiabatic evolution from the non-interacting Fermi gas by gradually turning on interactions. Although the ideal Fermi distribution function could be significantly distorted, its discontinuity remains which still defines a Fermi surface enclosing a volume in momentum space proportional to the total fermion number, as stated by the Luttinger theorem. Nevertheless the shape of the Fermi surface can be modified by interactions. The low energy excitations become the long-lived quasi-particles around the Fermi surface, whose life-time is inversely proportional to

the square of its energy due to the limited phase space for low energy scattering processes. The overlap between the quasi-particle state and the bare fermion state defines the wavefunction renormalization factor Z, which is suppressed from the non-interacting value of 1 but remains finite. Z is also the quasiparticle weight determining the discontinuity of the fermion occupation number at the Fermi surface.

The interactions among quasi-particles are captured by the phenomenological Landau interaction function, which describes the forward scattering processes of quasi-particles. The Landau interaction function can be decomposed into a set of Landau parameters F_l in which l denotes the partial wave channels. The physical observables, such as compressibility, specific heat and magnetic susceptibility, compared with their values in free Fermi gases, are renormalized by these Landau parameters.

The Fermi surface can be made analogues to an elastic membrane. The energy cost to deform the Fermi surface can be viewed as the surface tension, which consists of two contributions from the kinetic energy and the interaction energy. The kinetic energy cost is always positive, while the interaction part can be either positive or negative. If the Landau parameter F_l is negative and large, i.e. $F_l < -(2l+1)$, then the surface tension vanishes in this channel and then spontaneous distortion will develop on the Fermi surface [80]. This class of Fermi surface instability is denoted as Pomeranchuk instability in the literature. The simplest Pomeranchuk instability is ferromagnetism which is an instability in the s-wave spin channel.

The Landau interaction function also gives rise to collective excitations which are absent in free Fermi gases, such as the zero sound mode. The zero sound is a generalization of the sound waves in fluids and solids. In fluids, the sound wave describes the propagation of the density vibration $\rho(\vec{r}, t)$, which is a scalar wave; in solids the sound wave is the vibration of the displacements of atoms from their equilibrium positions $\vec{u}(\vec{r}, t)$, which is a vector wave. Compared to ordinary fluids which can only support density fluctuations, Fermi liquid possesses a microscopic structure of the Fermi surface which can be viewed as an elastic membrane, whose degree of freedom is infinite described by the spherical tensor variables δn_{lm}. Consider a macroscopically small and microscopically large volume around $\vec{r}$, around which a local Fermi surface can be defined. The local Fermi surface deformation can vibrate and propagate and thus generating sound waves $\delta n_{lm}(\vec{r}, t)$, which is the physical picture of the Fermi liquid collective excitations. The restoring force for the zero sound arises from Landau interactions rather than hydrodynamic collisions for the sound modes in ordinary fluids.

3.2. Single-particle properties

Let us neglect the influence of the confining trap and also assume that dipoles polarize along the z-axis. The second quantized Hamiltonian of a single component electric dipolar fermion system reads

$$H_d = \sum_{\vec{k}} [\epsilon(\vec{k}) - \mu] c^\dagger(\vec{k}) c(\vec{k}) + \frac{1}{2V_0} \sum_{\vec{k},\vec{k}',\vec{q}} V_d(\vec{q}) \times \psi^\dagger(\vec{k}+\vec{q}) \psi^\dagger(\vec{k}') \psi(\vec{k}'+\vec{q}) \psi(\vec{k}). \quad (12)$$

In section 3, we define the dimensionless parameter as $\lambda = d^2 m k_f/(3\pi^2\hbar^2)$. It describes the interaction strength, which equals the ratio between the average interaction energy and the Fermi energy up to a factor at the order of one.

The Fermi surface structure of an electric dipolar fermion system is uniform but anisotropic. Intuitively, the inter-particle distance along the z-axis is shorter than that along x and y-axes because the dipolar interaction is attractive (repulsive) along the z-(xy) direction, respectively. Consequently, the Fermi surface will be approximately a prolate ellipsoid, elongated along the z-axis and compressed in the equatorial xy-plane, which has been investigated in [31–34].

The above picture can be confirmed from the explicit calculation of the fermion self-energy at the Hartree–Fock level. The Hartree term vanishes because it involves the spatial average of the dipolar interaction. The anisotropy of the Fermi surface can be determined from the Fock term, while the latter also depends on the actual shape of the Fermi surface, thus they are coupled together and should be solved self-consistently. Nevertheless, at the leading order, we approximate the Fermi surface as a sphere with the radius in the free space as k_{f_0} and then $\Sigma^{\rm HF}(\vec{k})$ can be calculated analytically [34] as

$$\Sigma^{\rm HF}(\vec{k}) = -2\lambda E_{k_{f_0}} P_2(\cos\theta_k)\, I_{\rm 3D}\left(\frac{k}{k_{f_0}^{\rm 3D}}\right), \quad (13)$$

where $E_{k_{f_0}} = \frac{\hbar^2 k_{f_0}^2}{2m}$ and $I_{\rm 3D}(x) = \frac{\pi}{12}\{3x^2 + 8 - \frac{3}{x^2} + \frac{3(1-x^2)^3}{2x^3} \ln|\frac{1+x}{1-x}|\}$. In the two-component dipolar Fermi gases, the Hartree term still vanishes and the Fock term only exists for the intra-component interaction, thus the Hartree–Fock self-energy remains the same.

The anisotropic Fermi surface distortion is determined by solving the equation of chemical potential μ as

$$\epsilon_0(\vec{k}_f) + \Sigma^{\rm HF}(\vec{k}_f) = \mu(n, \lambda), \quad (14)$$

where n is the particle density. The Fermi wave vector $\vec{k}_f$ depends on the polar angle as

$$\frac{k_f(\theta_k)}{k_{f_0}} = 1 - \frac{4\pi^2}{45}\lambda^2 + \frac{2\pi}{3}\lambda P_2(\cos\theta_k), \quad (15)$$

in which the anisotropic distortion is at the linear order of λ and the λ^2 term appears to conserve the particle numbers. Although equation (15) is only valid at $\lambda \ll 1$, it provides qualitative features. The Fermi surface anisotropy was also calculated by using the numerical variational method in [31]. The comparison between the analytic perturbative result and the variational one is plotted in figure 2 for $\lambda = \frac{1}{2\pi}$. The Fermi surface based on the first order perturbation result equation (15) is less prolate than that based on the variational result.

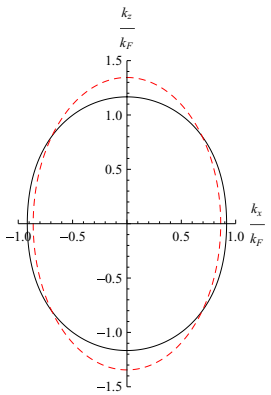

Figure 2. The deformed Fermi surface of the 3D dipolar system at $\lambda = \frac{1}{2\pi}$ by the perturbative (solid) and variational (dashed red) approaches. The external electric field lies along the z-axis. Reproduced from [34].

The anisotropy also exhibits in other single particle quantities. For example, the angular distribution of the density of states on the Fermi surface is calculated as

$$N(\Omega_k)\frac{\mathrm{d}\Omega_k}{4\pi} = \frac{mk_{f0}^{3\mathrm{D}}}{\hbar(2\pi)^3}\left[1+\frac{5\pi}{3}\lambda P_2(\cos\theta_k)\right]\mathrm{d}\Omega_k, \tag{16}$$

where, $N(\Omega_k)$ is the differential density of states along the direction of Ω_k. At the linear order of λ, $N(\Omega_k)$ develops the same anisotropy of $P_2(\cos\theta)$. Thus the total DOS at the Fermi energy does not change compared with that of the free Fermi gas. Nevertheless, it may be changed due to high order corrections.

3.3. The Landau interaction matrix

The anisotropic Fermi liquid theory has been constructed in [33, 34, 42] for the dipolar fermion systems. The anisotropy of the interaction leads to the mixing among different partial-wave channels, thus we need to generalize the concept of Landau parameters into the Landau matrices.

The variation of the Fermi distribution function at momentum $\vec{k}$ is defined as

$$\delta n_{\vec{k}} = n_{\vec{k}} - n_{0,k}, \tag{17}$$

where $n_0(k) = 1-\theta(k-k_{f_0}^{3\mathrm{D}})$ is the Fermi distribution function in the absence of interaction. The ground state energy variation of the single component dipolar Fermi gas is

$$\delta E = \sum_k \epsilon_k \delta n_k + \frac{1}{2V_0}\lim_{\vec{q}\to 0}\sum_{\vec{k},\vec{k}'} f(\vec{k},\vec{k}';\vec{q})\delta n_{\vec{k},\vec{q}}\delta n_{\vec{k},-\vec{q}}, \tag{18}$$

where, $\vec{k}$, $\vec{k}'$ are momenta close to the Fermi surface; $f(\vec{k},\vec{k}';\vec{q})$ is the interaction function describing the forward scattering; $\vec{q}$ is the small momentum transfer for the forward scattering process, which is explicitly kept because of the non-analyticity of the Fourier component of $V_d(\vec{q})$ as $\vec{q}\to 0$; $n_{\vec{k},\vec{q}} = \langle c^\dagger_{\vec{k}+\vec{q}} c_{\vec{k}}\rangle$, which is reduced to the fermion occupation number as $\vec{q}\to 0$; ϵ_k is the renormalized anisotropic single particle spectra and at the Hartree–Fock level $\epsilon_k = \epsilon_k^0 + \Sigma_{\mathrm{HF}}(\vec{k})$. The Landau interaction function is expressed at the Hartree–Fock level as

$$f(\vec{k},\vec{k}';\vec{q}) = V(\vec{q}) - V(\vec{k}-\vec{k}'), \tag{19}$$

where the first and second terms are the Hartree and Fock contributions, respectively. Due to the explicit anisotropy, $f(\vec{k},\vec{k}';\vec{q})$ depends on directions of both $\vec{k}$ and $\vec{k}'$, not just the relative angle between $\vec{k}$ and $\vec{k}'$ as in the isotropic Fermi liquids.

The Landau interaction matrix elements for the dipolar system have been calculated in [33] by Fregoso *et al* According to the Wigner–Eckart theorem, the $d_{r^2-3z^2}$ anisotropy of the dipolar interaction renders the following spherical harmonics decomposition as

$$f(\vec{k},\vec{k}';\vec{q}) = \sum_{l,l';m}\frac{4\pi f_{ll';m}}{\sqrt{(2l+1)(2l'+1)}}Y^*_{lm}(\Omega_k)Y_{l'm}(\Omega_{\vec{k}'}), \tag{20}$$

where $f_{ll';m}$ remains diagonal for the index m but couples partial wave channels with $l' = l, l\pm 2$. The even and odd partial wave channels decouple because of the even parity of the dipolar interaction. The $\vec{q}$ dependence only appear in the channel of $l = l' = m = 0$, in which $f_{00;0}(\vec{q}) = V_d(\vec{q})$. Other matrix elements at the Hartree–Fock level are tri-diagonal as[3]

$$f^{3\mathrm{D}}_{ll';m} = d^2\left(a^{(1)}_{lm}\delta_{l,l'} + a^{(2)}_{lm}\delta_{l,l'-2} + a^{(2)}_{l'm}\delta_{l',l-2}\right), \tag{21}$$

where

$$a^{(1)}_{lm} = \frac{4\pi(l^2+l-3m^2)(2l+1)}{l(l+1)(2l+3)(2l-1)},$$
$$a^{(2)}_{lm} = -\frac{2\pi\sqrt{[(l+1)^2-m^2][(l+2)^2-m^2]}}{(l+1)(l+2)(2l+3)}. \tag{22}$$

For each $l\neq 0$, $f^{3\mathrm{D}}_{ll';m}$'s satisfy the sum rule that

$$\sum_m f^{3\mathrm{D}}_{ll'=l;m} = 0, \tag{23}$$

which reflects the fact the angular average of the dipolar interaction vanishes.

To make the Landau matrix dimensionless, we multiply the single component density of states (DOS): $F^{3\mathrm{D}}_{ll';m} = \frac{m^*}{m}N_0^{3\mathrm{D}}f^{3\mathrm{D}}_{ll';m}$, where $N_0^{3\mathrm{D}} = (mk_{f0}^{3\mathrm{D}})/(2\hbar\pi^2)$ is the DOS of free Fermi gas and m^* is the effective mass. At the linear order of λ, $m^* = m$. For concreteness, some low order Landau matrix

[3] The expressions in equation (21) we use the standard normalization convention in [56] which is different from that in [33], thus the parameters in equation (22) are modified accordingly.

elements are expressed at the linear order of λ as

$$\begin{aligned} F_{00;0}(\Omega_{\vec{q}}) &= 4\pi\lambda P_2(\cos\theta_q), \\ F_{02;0} &= -\pi\lambda; \\ F_{22;0} = \frac{10\pi}{7}\lambda, &\quad F_{22;\pm1} = \frac{5\pi}{7}\lambda, \\ F_{22;\pm2} &= -\frac{10\pi}{7}\lambda; \\ F_{11;0} = \frac{18\pi}{5}\lambda, &\quad F_{11;\pm1} = -\frac{9\pi}{5}\lambda; \\ F_{13;0} = -\frac{3\pi}{5}\lambda, &\quad F_{13;\pm1} = -\frac{\sqrt{6}\pi}{5}\lambda; \\ F_{33;0} = \frac{14\pi}{15}\lambda, &\quad F_{33;\pm1} = \frac{7\pi}{10}\lambda; \\ F_{33;\pm2} = 0, &\quad F_{33;\pm3} = -\frac{7\pi}{6}\lambda. \end{aligned} \tag{24}$$

3.4. Thermodynamic quantities

The thermodynamic properties, including the anisotropic effective mass and thermodynamic susceptibilities, are renormalized by the Landau interaction matrices. For simplicity, only the single-component dipolar systems are considered here.

3.4.1. Anisotropic effective mass. It is well-known that the Galilean invariance leads to the relation between the bare mass of fermions and the effective mass of quasiparticles as [77, 78]

$$\frac{\vec{k}}{m} = \frac{\partial\epsilon(\vec{k})}{\partial\vec{k}} - \int \frac{\mathrm{d}^3\vec{k}'}{(2\pi)^3} f(\vec{k};\vec{k}')\frac{\partial n(\epsilon(\vec{k}'))}{\partial\vec{k}'}. \tag{25}$$

For an isotropic system, the effective mass m^* is defined as $\partial\epsilon(\vec{k})/\partial\vec{k} = \vec{k}/m^*$ for $\vec{k}$ on the Fermi surface. The renormalization of m^*, or, the renormalization of the density of states, is $\frac{m^*}{m} = 1 + \frac{1}{3}F_1^s$, which affects the specific heat as $C_{\mathrm{FL}}/C_{\mathrm{FG}} = m^*/m$, with C_{FL} and C_{FG} specific heats for the Fermi liquid and ideal Fermi gas, respectively.

The dipolar Fermi gas is Galilean invariant so that equation (25) is still valid. However, due to the anisotropy, a self-consistent solution has to be done numerically. To the linear order of λ, we approximate $\epsilon(\vec{k}')$ in the right-hand-side of equation (25) with the free fermion energy. Defining the radial effective mass as $m^*_{3\mathrm{D},\parallel}(\theta_k) = \frac{1}{k_f(\theta_k)}[\hat{k}\cdot\frac{\partial\epsilon(\vec{k})}{\partial\vec{k}}]$, we arrive at

$$\frac{1}{m} = \frac{1}{m^*_{3\mathrm{D},\parallel}(\theta_k)} + \frac{1}{m}\Big[\tilde{F}_{11,\parallel}(\theta_k) + \tilde{F}_{13,\parallel}(\theta_k)\Big], \tag{26}$$

where $\tilde{F}_{11,\parallel}(\theta_k)$ and $\tilde{F}_{13,\parallel}(\theta_k)$ are the angular dependent Landau parameters defined as follows

$$\begin{aligned} \tilde{F}_{11,\parallel}(\theta_k) &= \frac{4\pi}{3}\sum_m \frac{F_{11;m}}{3}|Y_{lm}(\theta_k,0)|^2 \\ \tilde{F}_{13,\parallel}(\theta_k) &= \frac{4\pi}{3}\sum_{m=0,\pm1}\frac{F_{13;m}}{\sqrt{21}}Y^*_{3m}(\theta_k,0)Y_{1m}(\theta_k,0). \end{aligned}$$

Thus to the linear order of λ, the anisotropic radial effective mass is

$$\frac{1}{m^*_{3\mathrm{D},\parallel}(\theta_k)} = \frac{1-\pi\lambda P_2(\cos\theta_k)}{m}. \tag{27}$$

3.4.2. Thermodynamic susceptibilities. Viewing the Fermi surface as an elastic membrane, we define the angular variation of the fermion distribution as

$$\delta n(\Omega_{\vec{k}}) = \int \frac{k^2\mathrm{d}k}{(2\pi)^3}\delta n_{\vec{k}}, \tag{28}$$

which can be further expanded in terms of the spherical harmonics as

$$\delta n(\Omega_{\vec{k}}) = \sum_{lm} Y_{lm}(\Omega_{\vec{k}})\delta n_{lm}. \tag{29}$$

For a Fermi surface distortion characterized by a set of δn_{lm}, the energy variation is calculated as

$$\frac{\delta E}{V} = 4\pi\Big\{\frac{1}{2\chi_0}\sum_{ll';m}\delta n^*_{lm}\delta n_{l'm}K^{3\mathrm{D}}_{ll';m} - h_{lm}\delta n_{lm}\Big\}, \tag{30}$$

where $\chi_0 = \frac{\bar{m}^*}{m}N_0$ is the density of states at the Fermi energy; $\bar{m}^*$ is the average value of the effective mass on the Fermi surface which equals m at the linear order of λ; $h_{lm} = h^{ex}_{lm} + h^0_{20}$. h^{ex}_{lm} is the external field in the partial wave channel of lm and $h^0_{20} = \frac{2}{3}\sqrt{\frac{\pi}{5}}\lambda E^{3\mathrm{D}}_{k_{f0}}$ is the explicit symmetry breaking arising from the dipolar interaction. The matrix kernel $K_{ll'}$ in equation (30) contains two parts as

$$K_{ll';m} = M_{ll';m} + \frac{F^{3\mathrm{D}}_{ll';m}}{\sqrt{(2l+1)(2l'+1)}}, \tag{31}$$

in which, $M_{ll';m}$ is the kinetic energy contribution. At the linear order of λ, $M_{ll';m}$ is calculated as

$$M^{3\mathrm{D}}_{ll';m} = m^{(1)}_{lm}\delta_{ll'} + m^{(2)}_{lm}\delta_{l,l'-2} + m^{(2)}_{lm}\delta_{l,l'-2},$$

where

$$\begin{aligned} m^{(1)}_{lm} &= 1 + \frac{l(l+1)}{4(2l+1)}a^{(1)}_{lm}\lambda, \\ m^{(2)}_{lm} &= \frac{3(l+1)(l+2)}{4\sqrt{(2l+1)(2l+5)}}a^{(2)}_{lm}\lambda. \end{aligned} \tag{32}$$

The expectation value of δn_{lm} in the field of h_{lm} can be straightforwardly calculated as

$$\delta n_{lm} = \chi_0(K^{3\mathrm{D}}_{ll';m})^{-1}h_{l'm}. \tag{33}$$

Thus $\chi_0(K^{3\mathrm{D}}_{ll';m})^{-1}$ is the renormalized susceptibility matrix for the 3D dipolar Fermi system [34].

3.4.3. Pomeranchuk stabilities. The inverse of an eigenvalue of the matrix $K_{ll';m}$ can be considered as a thermodynamical susceptibility in the corresponding eigen-channel. If all the eigenvalues of $K_{ll';m}$ are positive, i.e. this matrix is positive-definite, then the system is thermodynamically stable. If any

of them becomes negative, the corresponding susceptibility diverges, which signals the onset of the Fermi surface instability of the Pomeranchuk type [34, 43]. For the isotropic system, $K_{ll';m}$ is already diagonal and m-independent and the criterion for the Pomeranchuk instability is the well-known one

$$F_l < -(2l+1). \tag{34}$$

For the anisotropic dipolar system, the $K_{ll';m}$ matrix needs to be diagonalized to analyze its thermodynamic instabilities. The two strongest instabilities lie in the sectors of of $m = 0$ and $m = \pm 2$ and l's are even. For the case of $m = 0$, $F_{00;0}(\vec{q})$ is singular as $\vec{q} \to 0$, explicitly depending on the direction of $\vec{q}$. The most negative eigenvalue occurs when $\vec{q}$ lies in the equatorial plane. The corresponding eigenvector mainly lies in the s-wave channel with $l = 0$ and the eigenvalue μ_s reaches zero at $\lambda_s = 0.135$. This instability corresponds to the Fermi surface collapsing with a density modulation wave vector in the equatorial plane. This result nicely agrees with the numerical calculation in [36], in which the onset of an unstable collective mode implies the Fermi surface collapsing starting from $\lambda_s \sim 0.14$. It should be noted that, actually, this instability is mostly driven by the Hartree term interaction $V_d(\vec{q})$, which cannot be simply dropped off by setting $\vec{q} = 0$. Otherwise, the stability of the dipolar Fermi gas would be significantly overestimated.

As for the sector of $m = \pm 2$, the eigenvectors of the minimal eigenvalues mainly lie in the $d_{x^2-y^2\pm 2ixy}$-wave channels. The lowest eigenvalues $\mu_{d_{\pm 2}}$ touch zero at $\lambda_{d_{\pm 2}} = 0.35$. This instability corresponds to the biaxial nematic instability of the Fermi surfaces studied in [43]. With the purely dipolar interaction, the s-wave channel instability occurs before the d-wave channel one because $\lambda_{d\pm 2} > \lambda_s$. Nevertheless, the s-wave channel instability can be cured by introducing a positive non-dipolar short-range s-wave scattering potential $V_{00;0}$, which adds to the Landau parameter of $F^{3D}_{00;0}$ without affecting other channels.

3.5. The collective zero sound mode

In this part, we review the calculation of the zero-sound-like collective mode in the dipolar Fermi gases [34, 36]. The anisotropic dipolar interaction brings a new feature: the zero sound excitation can only propagate within a certain range of directions beyond which the sound mode is damped.

3.5.1. Generalized dynamical response functions. The Boltzmann equation for the collective excitation of the single-component Fermi liquid is [79]

$$\frac{\partial}{\partial t} n(\vec{r},\vec{k},t) + \sum_i \frac{\partial \epsilon(\vec{r},\vec{k},t)}{\partial k_i}\frac{\partial n(\vec{r},\vec{k},t)}{\partial r_i} - \sum_i \frac{\partial \epsilon(\vec{r},\vec{k},t)}{\partial r_i}\frac{\partial n(\vec{r},\vec{k},t)}{\partial k_i} = 0, \tag{35}$$

where $n(\vec{r},\vec{k},t)$ and $\epsilon(\vec{r},\vec{k},t)$ are the density and energy distributions in the phase space.

In order to linearize the Boltzmann equation, the small variations of $n(\vec{r},\vec{k},t)$ and $\epsilon(\vec{r},\vec{k},t)$ are defined as

$$\begin{aligned} n(\vec{r},\vec{k},t) &= n_{0,d}(k) + \delta\nu(\vec{r},\vec{k},t), \\ \epsilon(\vec{r},\vec{k},t) &= \epsilon_{\rm HF}(k) + \int \frac{{\rm d}^3k'}{(2\pi)^3} f(\hat{k},\hat{k}')\delta\nu(\vec{r},\hat{k}',t), \end{aligned} \tag{36}$$

where $\delta\nu$ is defined with respect to the deformed equilibrium Fermi surface and $\epsilon_{\rm HF}$ is the Hartree–Fock single particle spectrum. Substituting $\delta\nu(\vec{r},\vec{k},t) = \sum_q \delta\nu_{\vec{k}} {\rm e}^{{\rm i}(\vec{q}\cdot\vec{r}-\omega t)}$, the linearized Boltzmann equation is arrived at

$$\delta\nu(\Omega_k) - \frac{N(\Omega_k)\vec{v}_{\vec{k}}\cdot\vec{k}}{\omega - \vec{v}_{\vec{k}}\cdot\vec{q}} \int \frac{{\rm d}\Omega_{k'}}{4\pi} f_{\vec{k}\vec{k}'}\delta\vec{\nu}(\Omega_{k'}) = 0, \tag{37}$$

where $\vec{v}_{\vec{k}}$ is the Fermi velocity; $N(\Omega_k)$ is the differential density of states defined in equation (16); $\delta\nu(\Omega_k)$ is defined as

$$\delta\nu(\Omega_k) = \int \frac{k^2{\rm d}k}{(2\pi)^3}\delta\nu(\vec{k}). \tag{38}$$

The spherical harmonics decomposition can be performed as

$$\sum_{l'm'}\left\{\delta_{ll'}\delta_{mm'} + \sum_{l''}\chi_{ll'';mm'}(\omega,\vec{q})F_{l''l';m'}\right\}\delta\nu_{l'm'} = 0, \tag{39}$$

where $\delta\nu_{lm}$ is the component in terms of the spherical harmonics and,

$$\begin{aligned} \chi_{ll';mm'}(\omega,\vec{q}) = &-\frac{1}{\sqrt{(2l+1)(2l'+1)}}\int {\rm d}\Omega_p \frac{N^{\rm 3D}(\Omega_{\vec{p}})}{N_0^{\rm 3D}} \\ &\times Y^*_{lm}(\Omega_{\vec{p}})\frac{\vec{v}_p^{\rm 3D}.\vec{q}}{\omega - \vec{v}_p^{\rm 3D}.\vec{q}}Y_{l'm'}(\Omega_{\vec{p}}). \end{aligned} \tag{40}$$

Due to the dipolar anisotropy, for a general propagation direction of $\vec{q}$, $\delta\nu_{lm}$ in different channels are coupled.

3.5.2. The s-wave channel approximation. We first truncate equation (40) by only keeping the s-wave channel of $l = 0$. Even at this level, the anisotropy of the zero sound mode has already appeared. Taking into account the Hartree–Fock single particle spectra and the anisotropic Fermi surface, $\chi_{00;00}(\omega,\vec{q})$ is given by

$$\chi_{00;00}(\omega,\vec{q}) = 1 - \int \frac{{\rm d}\Omega_k}{4\pi}\frac{N(\Omega_k)}{N_0}\frac{s}{s - f(\Omega_k,\Omega_q) + {\rm i}\eta}, \tag{41}$$

where $f(\Omega_k,\Omega_q) = \frac{\vec{q}\cdot\nabla_k\epsilon_{\rm HF}(\vec{k})}{v_{f_0}q}$ and the propagation direction $\vec{q}$ is chosen in the xz-plane with the polar angle θ_q. Then the zero sound mode dispersion is determined by

$$1 + F_{00;0}(\Omega_{\vec{q}})\chi_{00;00}(\omega,\vec{q}) = 0. \tag{42}$$

The quantity $s(\theta_q) = \omega(\theta_q)/(v_{f_0}q)$ is defined to represent the angular dependent zero sound dispersion, which is solved numerically and plotted in figure 3 along with the edge of particle-hole continuum. The zero sound propagation angle is restricted and its dispersion $s(\theta_q)$ is anisotropic. For large angles of θ_q, the sound excitation enters the particle-hole continuum and is thus damped.

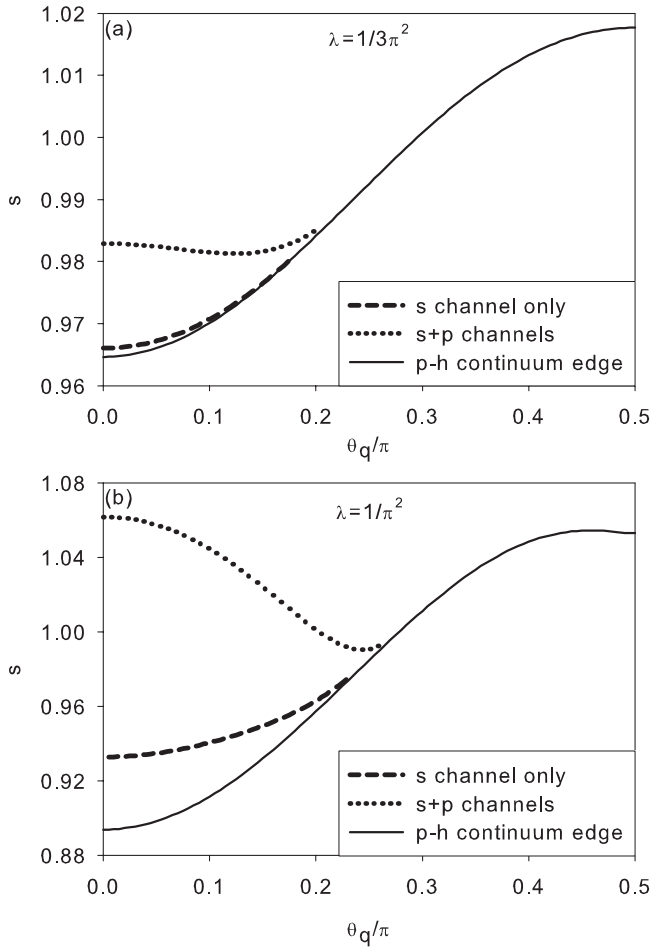

Figure 3. Dispersions of the zero sound $s(\theta_q) = \omega(\theta_q)/v_{f0}^{3D}q$ for the pure dipolar interaction at *a*) $\lambda = 1/(3\pi^2)$ and *b*) $\lambda = 1/\pi^2$. When the sound speed hits the particle hole continuum, the sound becomes damped. These results are in good agreement with the numerical study in [36]. Reproduced from [34].

3.5.3. Correction from the coupling to the p-wave longitudinal channel. Even in the isotropic Fermi liquid state, because the propagation direction $\vec{q}$ of the zero sound already breaks the 3D rotational symmetry to the uni-axial one, actually the zero sound mode mixes all the longitudinal channels of δn_{l0}. If the Landau parameter F_1 is not small compared to F_0, the mixing between the s and p-wave longitudinal channels significantly modifies the sound velocity. In the isotropic Fermi liquid state, the modified sound velocity is determined by the following equation as [79]

$$\frac{-1}{F_0 + \dfrac{s^2 F_1}{1 + \dfrac{F_1}{3}}} = 1 - \frac{s}{2}\ln\left|\frac{1+s}{1-s}\right|. \tag{43}$$

For example, in the ^{3}He system at 0.28 atm, if only considering the s-wave channel, the sound velocity is calculated as $s = v_s/v_f = 2.0$ based on $F_0^s = 10.8$. After including the coupling of the p-wave longitudinal channel in which $F_1^s = 6.3$, the revised value of s increases to 3.6 in agreement with the experimental measurements [79].

The case of the dipolar Fermi gas is more complicated. If the propagating direction $\vec{q}$ is not along the z-axis, no rotational symmetry is left and thus, in principle, the longitudinal and transverse p-wave components are mixed. Here, the spherical harmonic functions $\tilde{Y}_{l=1,m=0}$ (longitudinal) and $\tilde{Y}_{l=1,m=\pm1}$ (transverse) are defined according to the principle axis along $\vec{q}$ instead of the z-axis. Nevertheless, usually the transverse p-wave channel mode is overdamped unless the p-wave channel Landau parameter is positive and large, thus their effect to the zero sound mode is small and will be neglected.

By keeping the mixing between the s-wave and the longitudinal p-wave modes, equation (40) is reduced to a 2×2 matrix equation and the collective mode can be solved based on

$$\mathrm{Det}[1 + N(\vec{q},\omega)] = 0, \tag{44}$$

where the matrix kernel of $N(\vec{q},\omega)$ reads

$$N(\vec{q},\omega) = \begin{pmatrix} \chi_{00;00}(\vec{q},\omega)F_{00;0}(\vec{q}) & \tilde{\chi}_{10;00}(\vec{q},\omega)\frac{\tilde{F}_{110}(\vec{q})}{3} \\ \tilde{\chi}_{10;00}(\vec{q},\omega)F_{00;0}(\vec{q}) & \tilde{\chi}_{11;00}(\vec{q},\omega)\frac{\tilde{F}_{11;0}(\vec{q})}{3} \end{pmatrix}. \tag{45}$$

$\tilde{F}_{11;0}^{3D}(\vec{q})$ is the longitudinal p-wave Landau parameter defined as

$$\tilde{F}_{11;0}(\vec{q}) = \cos^2\theta_q F_{11;m=0} + \sin^2\theta_q F_{11;m=\mp1}, \tag{46}$$

and the response functions are

$$\tilde{\chi}_{10;00}(\vec{q},\omega) = -\sqrt{3}\int \frac{\mathrm{d}\Omega_k}{4\pi}\frac{N(\Omega_k)}{N_0}\frac{(\hat{q}\cdot\hat{k})f(\Omega_k,\Omega_q)}{s - f(\Omega_k,\Omega_q)},$$

$$\tilde{\chi}_{11;00}(\vec{q},\omega) = -3\int \frac{\mathrm{d}\Omega_k}{4\pi}\frac{N(\Omega_k)}{N_0}\frac{(\hat{q}\cdot\hat{k})^2 f(\Omega_k,\Omega_q)}{s - f(\Omega_k,\Omega_q)},$$

where $\vec{q}$ lies in the xz-plane with the polar angle θ_q and $\hat{q}\cdot\hat{k} = \sin\theta_q\sin\theta_k\cos\phi_k + \cos\theta_q\cos\theta_k$.

The numeric solution taking into account the anisotropic Fermi velocity and Fermi surface is performed and the zero sound velocity as a function of θ_q is plotted in figure 3. The longitudinal p-wave mode modifies the sound velocity dispersion significantly. These results are in a good agreement with a fully numerical calculation based on the same Boltzmann transport theory [36]. This indicates that the zero sound mode is well captured by the coupling between the s-wave and longitudinal p-wave channels.

4. The SO coupled Fermi liquid theory of the magnetic dipolar fermions

The magnetic dipolar interaction brings a new ingredient to the Fermi liquid theory, i.e. the SO coupled nature [43, 58–65]. Certainly, for the experimental system of the ^{161}Dy atoms whose hyperfine spin is as large as $F = \frac{21}{2}$ [21, 26, 27], the theoretical analysis on magnetic dipolar interactions will be very challenging. Nevertheless, the spin-$\frac{1}{2}$ case exhibits nearly all the qualitative features of the magnetic dipolar interaction and thus will be used as a prototype model below.

If the magnetic dipolar systems are partially polarized, this SO coupling already appears at the single-particle level

exhibiting anisotropic Fermi surfaces, which is a result from the ferro-nematic coupling as shown by Fregoso *et al* [43, 59]. For the unpolarized case, the Fermi surfaces remain spherical without splitting. Nevertheless, the effects of the SO coupling appear at the interaction level [61, 62], including Fermi surface Pomeranchuk instabilities and SO coupled collective modes.

The second quantized Hamiltonian of the spin-$\frac{1}{2}$ fermions with the magnetic dipolar interaction is expressed as

$$H_{md} = \sum_{\vec{k},\alpha}[\epsilon(\vec{k}) - \mu]c^{\dagger}_{\alpha}(\vec{k})c_{\alpha}(\vec{k}) + \frac{1}{2V_0}\sum_{\vec{k},\vec{k}',\vec{q}} V_{\alpha\beta;\beta'\alpha'}(\vec{q}) \times \psi^{\dagger}_{\alpha}(\vec{k}+\vec{q})\psi^{\dagger}_{\beta}(\vec{k}')\psi_{\beta'}(\vec{k}'+\vec{q})\psi_{\alpha'}(\vec{k}). \quad (47)$$

Similarly, the dimensionless interaction parameter can be defined accordingly as $\lambda_m = \mu_B^2 g_F^2 m k_f/(\pi^2\hbar^2)$.

The SO coupled Landau interaction function is reviewed and the SO coupled partial wave decomposition is performed in section 4.1; the Pomeranchuk instability is reviewed in section 4.2; the zero sound-like excitation with the SO coupled feature is reviewed in section 4.3.

4.1. The SO coupled Landau interaction

In [61], the Landau interaction function of the magnetic dipolar fermions with a general hyperfine-spin F was given. For simplicity and concreteness, below we still use the spin-$\frac{1}{2}$ case for illustration [62]. Based on the Fourier transform of the magnetic dipolar interaction equation (11), the Landau function of the spin-$\frac{1}{2}$ magnetic dipolar system is expressed at the Hartree–Fock level as

$$f_{\alpha\alpha',\beta\beta'}(\vec{k},\vec{k}';\vec{q}) = f^{H}_{\alpha\alpha',\beta\beta'}(\hat{q}) + f^{F}_{\alpha\alpha',\beta\beta'}(\vec{k},\vec{k}') = \frac{\pi g_F^2\mu_B^2}{3}\big(M_{\alpha\alpha',\beta\beta'}(\hat{q}) - M_{\alpha\alpha',\beta\beta'}(\hat{p})\big),$$

where $\vec{k}$ and $\vec{k}'$ are at the Fermi surface; the small momentum transfer $\vec{q}$ in the Hartree term is explicitly kept due to the singularity at $\vec{q}\to 0$ in equation (11); $\hat{p}$ is the unit vector defined as $\hat{p} = \frac{\vec{k}-\vec{k}'}{|\vec{k}-\vec{k}'|}$; the matrix kernel $M_{\alpha\alpha',\beta\beta'}(\hat{m})$ only depends on the direction of $\hat{m}$ as

$$M_{\alpha\alpha',\beta\beta'}(\hat{m}) = 3(\vec{\sigma}_{\alpha\alpha'}\cdot\hat{m})(\vec{\sigma}_{\beta\beta'}\cdot\hat{m}) - \vec{\sigma}_{\alpha\alpha'}\cdot\vec{\sigma}_{\beta\beta'}, \quad (48)$$

for $\hat{m} = \hat{p}$ and $\hat{q}$. In order to arrive at $f^{F}_{\alpha\alpha',\beta\beta'}(\vec{k},\vec{k}')$ in equation (48), the following identity is used

$$3(\vec{\sigma}_{\alpha\beta'}\cdot\hat{p})(\vec{\sigma}_{\beta\alpha'}\cdot\hat{p}) - \vec{\sigma}_{\alpha\beta'}\cdot\vec{\sigma}_{\beta\alpha'} = 3(\vec{\sigma}_{\alpha\alpha'}\cdot\hat{p})(\vec{\sigma}_{\beta\beta'}\cdot\hat{p}) - \vec{\sigma}_{\alpha\alpha'}\cdot\vec{\sigma}_{\beta\beta'}. \quad (49)$$

4.1.1. The SO partial-wave decomposition. It is convenient to work in the SO coupled bases for the magnetic dipolar Fermi liquid theory. The variation of the single particle density matrix in momentum space is defined as $\delta n_{\alpha\alpha'}(\vec{k}) = n_{\alpha\alpha'}(\vec{k}) - \delta_{\alpha\alpha'}n_0(\vec{k})$, where $n_{\alpha\alpha'}(\vec{k}) = \langle\psi^{\dagger}_{\alpha}(\vec{k})\psi_{\alpha'}(\vec{k})\rangle$ and $n_0(\vec{k})$ refers to the ground state distribution of the free Fermi system. As for spin indices, $\delta n_{\alpha\alpha'}(\vec{k})$ can be expanded as

$$\delta n_{\alpha\alpha'}(\vec{k}) = \sum_{Ss_z}\delta n_{Ss_z}(\vec{k})\chi_{Ss_z,\alpha\alpha'}, \quad (50)$$

where $\chi_{Ss_z,\alpha\alpha'}$ are the bases for the particle-hole singlet (density) channel with $S=0$ and triplet (spin) channel with $S=1$, respectively, defined as

$$\chi_{10,\alpha\alpha'} = \sigma_{z,\alpha\alpha'},\quad \chi_{1\pm1,\alpha\alpha'} = \frac{\mp1}{\sqrt{2}}(\sigma_{x,\alpha\alpha'} \pm i\sigma_{y,\alpha\alpha'}),\quad \chi_{00,\alpha\alpha'} = \delta_{\alpha\alpha'}. \quad (51)$$

Similarly as before, we integrate $\delta n_{\alpha\alpha'}(\vec{k})$ along the radial direction and arrive the angular distribution $\delta n_{\alpha\alpha'}(\hat{k})$. In the SO decoupled bases, it is expanded as

$$\delta n_{\alpha\alpha'}(\hat{k}) = \sum_{LmSs_z}\delta n_{LmSs_z}Y_{Lm}(\hat{k})\chi_{Ss_z,\alpha\alpha'}. \quad (52)$$

More conveniently, it can be reorganized in the SO coupled bases as

$$\delta n_{\alpha\alpha'}(\hat{k}) = \sum_{JJ_z;LS}\delta n_{JJ_z;LS}\,\mathcal{Y}_{JJ_z;LS}(\hat{k},\alpha\alpha'), \quad (53)$$

where $\delta n_{JJz;LS} = \sum_{ms_z}\langle LmSs_z|JJ_z\rangle\delta n_{LmSs_z}$; $\mathcal{Y}_{JJz;LS}(\hat{k},\alpha\alpha')$ is the SO coupled spherical harmonic functions

$$\mathcal{Y}_{JJz;LS}(\hat{k},\alpha\alpha') = \sum_{ms_z}\langle LmSs_z|JJ_z\rangle Y_{Lm}(\hat{k})\chi_{Ss_z,\alpha\alpha'}.$$

Using the SO coupled bases, the Landau matrix is diagonal with respect to the total angular momentum J and its z-component J_z as

$$\frac{N_0}{4\pi}f_{\alpha\alpha';\beta\beta'}(\hat{k},\hat{k}') = \sum_{JJ_zLL'}\mathcal{Y}_{JJz;L1}(\hat{k},\alpha\alpha')F_{JJ_zL1;JJ_zL'1} \times\mathcal{Y}^{\dagger}_{JJz;L'1}(\hat{k},\beta\beta'). \quad (54)$$

The matrix kernel $F_{JJ_zL1;JJ_zL'1}$ reads

$$F_{JJ_zL1;JJ_zL'1} = \frac{\pi\lambda}{3}\delta_{J,1}\delta_{L,0}\delta_{L',0}(2\delta_{J_z,0} - \delta_{J_z,\pm1}) + \sum_{ms_z;m's'_z}\langle Lm1s_z|JJ_z\rangle\langle L'm'1s'_z|JJ_z\rangle T^{F}_{Lm1s_z;L'm'1s'_z}, \quad (55)$$

in which the first term is the Hartree contribution with $\hat{q}$ set as the z-axis; the second term is the Fock contribution with $T^{F}_{Lm1s_z;L'm'1s'_z}$ defined in the SO decoupled bases as [61, 62]

$$T^{F}_{Lm1s_z;L'm'1s'_z} = -\frac{\pi\lambda}{2}\Big(\frac{\delta_{LL'}}{L(L+1)} - \frac{\delta_{L+2,L'}}{3(L+1)(L+2)} - \frac{\delta_{L-2,L'}}{3(L-1)L}\Big)\int d\Omega_r\Big(\delta_{s_zs'_z} - 4\pi Y_{1s_z}(\Omega_r)Y^{*}_{1s'_z}(\Omega_r)\Big) \times Y_{Lm}(\Omega_r)Y^{*}_{L'm'}(\Omega_r). \quad (56)$$

The same value of J may arise from L with different parities. Below we use $(J^{\pm}J_zLS)$ to represent different angular momentum channels, where $\pm$ is the parity eigenvalue. The Hartree term of equation (55) only contributes to the (1^+J_z01) sector, which explicitly depends on J_z because $\vec{q}$ (chosen as the $\hat{z}$-axis) breaks the 3D rotation symmetry down to the uniaxial rotation symmetry. For other sectors, $F_{J^{\pm}J_zL1;J^{\pm}J_zL'1}$ does not depend on J_z as required by the Wigner–Eckart theorem. The matrix $F_{JJ_zL1;JJ_zL'1}$ is nearly diagonalized except for the case with $L\neq L'$. For $J^+ = 0^+, 2^+, ..$ and $J^- = 1^-, 3^-, ...$, there is only one possibility

that $L = J$ and thus $F_{J^{\pm}J_zL1;J^{\pm}J_zL'1}$ is already diagonalized. In comparison, for $J^+ = 1^+, 3^+, ...$ and $J^- = 0^-, 2^-, ...$ L can take two different values of $L = J \pm 1$ and thus the matrix is reduced to 2×2 (For $J^- = 0^-$ the only possibility is $L = 1$.). The concrete forms of $F_{J^{\pm}J_zL1;J^{\pm}J_zL'1}$ for a few low orders of $J^{\pm}$ are given in [61, 62].

4.1.2. Thermodynamics susceptibilities. The variation of the ground state energy in the SO coupled bases is expressed as

$$\frac{\delta E}{V} = 16\pi \Big\{ \frac{1}{2\chi_0} \sum_{JJ_zLL'S} \delta n^*_{JJ_z;LS} M_{JJ_zLS;JJ_zL'S} \delta n_{JJ_z;L'S} - \sum_{JJ_zLS} h_{JJ_zLS} \delta n_{JJ_z;LS} \Big\}, \quad (57)$$

where the matrix kernel is

$$M_{JJ_zLS;JJ_zL'S} = \delta_{LL'} + F_{JJ_zLS;JJ_zL'S}; \quad (58)$$

$\chi_0 = N_0$ is the Fermi liquid density of states; h_{JJ_zLS} is the external field. At the Hartree–Fock level, N_0 receives no renormalization from the magnetic dipolar interaction. The expectation value of δn_{JJ_zLS} is calculated as

$$\delta n_{JJ_zLS} = \chi_0 \sum_{L'} (M)^{-1}_{JJ_zLS;JJ_zL'S} h_{JJ_zL'S}. \quad (59)$$

The thermodynamic stability condition is equivalent to that all the eigenvalues of the matrix $M_{JJ_zLS;JJ_zL'S}$ are positive.

Fregoso *et al* [43, 59] found that a uniform magnetic field $\vec{h}$ along the z-axis not only induces spin polarization, but also a spin-nematic order in the channel of $(J^+J_zLS) = (1^+021)$. As a result, the external magnetic field induces an effective SO coupling

$$H_{\rm hso} = \frac{\sqrt{2}}{12}\pi\lambda h \sum_k \psi^{\dagger}_{\alpha}(\vec{k}) \Big\{ \big[(k^2 - 3k_z^2)\sigma_z - 3k_z(k_x\sigma_x + k_y\sigma_y) \big] \Big\} \psi_{\beta}(\vec{k}). \quad (60)$$

Apparently, equation (60) breaks TR symmetry, which is markedly different from the relativistic SO coupling in solids.

4.2. SO coupled Pomeranchuk instabilities

If one of the eigenvalue of the Landau matrix becomes negative, Pomeranchuk instability occurs in the corresponding channel. The SO coupled nature in the magnetic dipolar system manifests as follows.

Let us first consider the channel of $J = 1^+$ [62]. In the absence of external fields, a density wave with a long wave length $q \to 0$ can take the advantage of the Hartree channel interaction. The leading instability lies in the sector with $J_z = \pm 1$. Without loss of generality, we use the $J_z = 1$ sector as an example:

$$\begin{pmatrix} F_{1101;1101} & F_{1101;1121} \\ F_{1121;1101} & F_{1121;1121} \end{pmatrix} = \frac{\pi\lambda_m}{12} \begin{pmatrix} -4 & \sqrt{2} \\ \sqrt{2} & 1 \end{pmatrix}, \quad (61)$$

whose negative eigenvalue and the associated eigenvector are

$$w_1^{1^+1} = -0.37\pi\lambda_m, \quad \psi_1^{1^+1} = (0.97, -0.25)^T. \quad (62)$$

The instability occurs at $w_1^{1^+1} < -1$, or, equivalently, $\lambda_m > \lambda^c_{1^+1} = 0.86$ and the eigenvector shows that it is nearly a ferromagnetic instability hybridized with a small component of the ferro-nematic channel. The spin polarizations lie in the xy-plane and the spiral wave vector is along the z-axis. The spiral wave vector $\vec{q}$ should be at the order of the inverse of the system size in order to minimize the energy cost of spin twisting, which may further depend on concrete boundary conditions.

An interesting point is that because of the coupling between the ferromagnetic and ferro-nematic orders, the Fermi surfaces are distorted [59]. The oscillations of the distorted Fermi surfaces couple to spin waves and bring Landau damping to spin waves. This may result in non-Fermi liquid behavior to fermion excitations. Similar effects in the nematic Fermi liquid state have been extensively studied before in the literature [81–83].

The next sub-leading instability is in the $J = 1^-$ channel with $L = 1$ and $S = 1$, which has been studied in [61, 62]. For $J_z = 0$, the generated SO coupling at the single particle level exhibits the 3D Rashba-type as

$$H_{\rm so,1^-} = |n_z| \sum_k \psi^{\dagger}_{\alpha}(\vec{k})(k_x\sigma_y - k_y\sigma_x)_{\alpha\beta}\psi_{\beta}(\vec{k}), \quad (63)$$

where $|n_z|$ is the magnitude of the SO order parameter. The magnetic dipolar interaction already possesses the SO nature. The Pomeranchuk instability brings it to the single particle level by breaking rotational symmetry and parity.

The instability of the $J = 1^-$ sector is similar to but fundamentally different from the Pomeranchuk instability in the $L = S = 1$ channel studied in [84, 85]. Different from the magnetic dipolar systems, the starting Hamiltonian in the latter case has no SO coupling at all. After instability occurs, an effective SO coupling appears at the single particle level. In particular, a $\vec{k} \cdot \vec{\sigma}$ type SO coupling can be generated with total angular momentum $J = 0$. It is generated from the SO decoupled interactions through a phase transition and thus was denoted as spontaneous generation of SO coupling [84, 85]. They are a particle-hole channel analogy of the p-wave triplet Cooper pairings of the isotropic ^{3}He-B phase [86] and the anisotropic ^{3}He-A-phase [87, 88], respectively.

4.3. The SO coupled collective modes: the topological zero sound

We review the study of the collective modes in the SO coupled Fermi liquid theory [61, 62]. The generalized Boltzmann equation including the spin degree of freedom can be written as [79]

$$\frac{\partial}{\partial t} n(\vec{r},\vec{k},t) - \frac{i}{\hbar}[\epsilon(\vec{r},\vec{k},t), n(\vec{r},\vec{k},t)] + \frac{1}{2}\sum_i \Big\{ \frac{\partial \epsilon(\vec{r},\vec{k},t)}{\partial k_i}, \frac{\partial n(\vec{r},\vec{k},t)}{\partial r_i} \Big\} - \frac{1}{2}\sum_i \Big\{ \frac{\partial \epsilon(\vec{r},\vec{k},t)}{\partial r_i}, \frac{\partial n(\vec{r},\vec{k},t)}{\partial k_i} \Big\} = 0, \quad (64)$$

where $n_{\alpha\alpha'}(\vec{r},\vec{k},t)$ and $\epsilon_{\alpha\alpha'}(\vec{r},\vec{k},t)$ are the density and energy matrices for the coordinate $(\vec{r},\vec{k})$ in the phase space; [,] and

{, } mean the commutator and anti-commutator, respectively. After linearizing equation (64) and expanding it in the plane-wave bases

$$\delta n_{\alpha\alpha'}(\vec{r},\vec{k}) = \sum_{q} \delta n_{\alpha\alpha'}(\vec{k}) e^{i\vec{q}\cdot\vec{r}-i\omega t}, \tag{65}$$

we arrive at

$$\delta n_{\alpha\alpha'}(\hat{k}) - \frac{1}{2}\frac{\cos\theta_k}{s-\cos\theta_k}\sum_{\beta\beta'}\int d\Omega_{k'}\frac{N_0}{4\pi} f_{\alpha\alpha',\beta\beta'}(\hat{k},\hat{k}') \times \delta n_{\beta\beta'}(\hat{k}') = 0, \tag{66}$$

where s is the dimensionless parameter $\omega/(v_f q)$. Without loss of generality, the propagation direction of the wave vector $\vec{q}$ is defined as the z-direction.

By using the SO coupled bases $\delta n_{JJ_z;LS}$, equation (66) is rewritten as

$$\delta n_{JJ_z;LS} + \sum_{J';LL'} K_{JJ_zLS;J'J_zL'S}(s) F_{J'J_zL'S;J'J_zL''S} \times \delta n_{J'J_zL''S} = 0, \tag{67}$$

The matrix kernel $K_{JJ_zLS;J'J_zL'S}$ reads

$$K_{JJ_zLS;J'J_zL'S}(s) = \sum_{ms_z}\langle LmSs_z|JJ_z\rangle\langle L'mSs_z|J'J_z\rangle \times \Omega_{LL';m}(s), \tag{68}$$

where $\Omega_{LL'}(s)$ is equivalent to the particle-hole channel Fermi bubble in the diagrammatic method defined as

$$\Omega_{LL';m}(s) = -\int d\Omega_{\hat{k}} Y^*_{Lm}(\hat{k}) Y_{L'm}(\hat{k}) \frac{\cos\theta_k}{s-\cos\theta_k}. \tag{69}$$

The largest positive Landau parameter lies in the (1^+001) channel, which can support propagating modes. Since $\vec{q}$ breaks parity and the 3D rotation symmetries, the (1^+001) channel couples to other channels with $J_z = 0$. The Landau parameters of orbital partial wave channels with $L \geqslant 2$ are small, which will be neglected henceforth. There are three spin channel modes with $L = S = 1$ and $J_z = 0$ denoted as (0^-011), (1^-011) and (2^-011). Even in the presence of $\vec{q}$, the system still possesses the reflection symmetry with respect to any plane including $\vec{q}$. By writing down their bilinear fermion expressions, we can check that among the above modes, (1^+001), (0^-011), (2^-011) are odd and (1^-011) is even under this reflection operation. Furthermore, the (2^-011) channel can be neglected because the Landau parameter in this channel is about one order smaller than those in (1^+001) and (0^-011).

Now, we only keep two coupled modes (1^+001) and (0^-011). Using the following relations

$$\begin{aligned} K_{1001;1001}(s) &= \Omega_{00;0}(s), \\ K_{1001;0011}(s) &= K_{0011;1001}(s) = s\Omega_{00;0}(s), \\ K_{0011,0011}(s) &= \sum_m |\langle 1m1-m|00\rangle|^2 \Omega_{11;m}(s) \\ &= \Omega_{00;0}(s), \end{aligned} \tag{70}$$

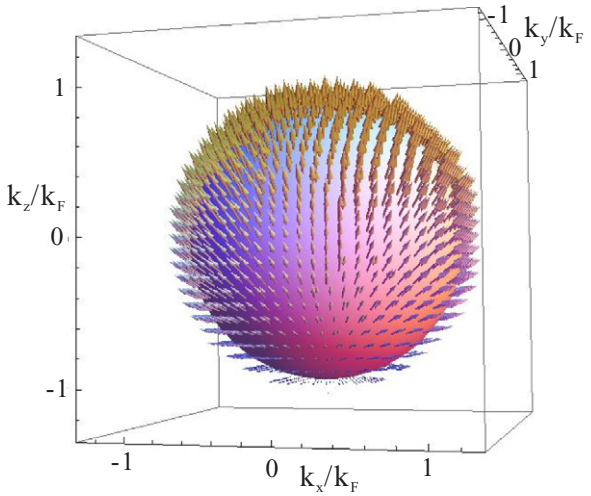

Figure 4. The spin configuration (equation (72)) of the zero sound mode over the Fermi surface shows the hedgehog type topology. Although the hedgehog configuration is distorted in the z-component, its topology does not change for any values of λ_m describing the interaction strength. Reproduced from [89].

we reduce the coupled 2×2 matrix equation based on equation (67) into

$$\begin{aligned} \Omega_{00;0}(s) &= 1 - \frac{s}{2}\ln\left|\frac{1+s}{1-s}\right| + i\frac{\pi}{2}s\Theta(s<1) \\ &= \frac{F_+ \pm \sqrt{F_+^2 + 4(s^2-1)F_\times}}{2(s^2-1)F_\times}, \end{aligned} \tag{71}$$

where

$$F_+ = F_{1001:1001} + F_{0011;0011},\ F_\times = F_{1001:1001}F_{0011;0011}.$$

For the two branches of equation (71), only the one with the minus sign possesses the solution with $s > 1$, as required by the condition of the undamped collective mode of the Fermi liquid. Since $n_{1^+001}(\vec{q}) = \sum_{\vec{k}} \psi^\dagger(\vec{k}+\vec{q})\sigma_z\psi_\beta(\vec{k})$ and $n_{0^-011}(\vec{q}) = \sum_{\vec{k}} \psi^\dagger(\vec{k}+\vec{q})(\vec{k}\cdot\vec{\sigma})\psi_\beta(\vec{k})$, the former mode describes spin oscillation along the direction of $\vec{q}$ and the latter exhibits a hedgehog configuration of spin distribution on the Fermi surface. The eigen-mode is a hybridization between them, which can be represented as

$$\vec{s}(\vec{r},\vec{k},t) = \begin{pmatrix} u_2\sin\theta_{\vec{k}}\cos\phi_{\vec{k}} \\ u_2\sin\theta_{\vec{k}}\sin\phi_{\vec{k}} \\ u_2\cos\theta_{\vec{k}} + u_1 \end{pmatrix} e^{i(\vec{q}\cdot\vec{r}-sqv_f t)}, \tag{72}$$

where $(u_1, u_2)^T$ is the eigenvector for the collective mode. For all the values of λ_m, $|u_2| > |u_1|$ is satisfied. Thus, the spin configuration, as shown in figure 4, is topologically non-trivial with the Pontryagin index ± 1. The sign of the Pontryagin index periodically flips at the nodes of the sound wave as the time and spatial coordinates varies. This collective mode can be considered as the topological zero sound.

5. Unconventional triplet Cooper pairing with multi-component dipolar Fermi gases

The p-wave ($L = 1$) triplet ($S = 1$) Cooper pairing is a celebrated unconventional pairing superfluid state which has

been a research focus of condensed matter physics for decades (see [56, 90] for reviews). The typical system is the superfluid ^{3}He which exhibits both the isotropic B phase [86] and the anisotropic A-phase [87, 88]. So far, the most accepted pairing mechanism is spin fluctuations arising from the prominent ferromagnetic tendency because there exists a hard core part in the interaction between two ^{3}He atoms.

As explained in section 1, the anisotropic dipolar interaction provides a novel and robust mechanism for the p-wave spin triplet Cooper pairing and the competition between the singlet and triplet channel pairing instabilities [28, 29, 44–54, 69]. Furthermore, the coexistence of the singlet and triplet pairing symmetries in the electric dipolar systems naturally leads to a novel TR symmetry breaking mechanism first pointed out in [50]. Recently, this mechanism is also studied in a wide context of superconducting systems [91, 92]. For example, it has been later proposed in the iron-based superconductors [92] and its topological electro-magnetic responses have been also studied [91]. In fact, the TR symmetry breaking pairing is also a research focus in condensed matter physics, such as in the study of high T_c cuprates (e.g. $YBa_2Cu_3O_{6+x}$) [93] and ruthenates (e.g. Sr_2RuO_4) [94].

In this section, we will first present a brief overview of the p-wave pairing in the superfluid ^{3}He system in section 5.1. The pairing symmetries in the single-component and two-component electric dipolar fermion systems are reviewed in section 5.2 and section 5.3, respectively. The effect of the TR reversal symmetry breaking is reviewed in section 5.4.

5.1. A quick overview of the p-wave triplet pairing in the superfluid ^{3}He system

The general structure of the p-wave spin triplet pairing takes the form of a 2×2 symmetric matrix $\Delta_{\alpha\beta}(\vec{k})$ in momentum space, which can be conveniently represented by the d-vector as [56]

$$\Delta_{\alpha\beta}(\vec{k}) = \Delta(\vec{k})\hat{d}_\mu(\vec{k})(\mathrm{i}\sigma^\mu\sigma^y)_{\alpha\beta}, \tag{73}$$

where $\Delta(\vec{k})$ is a complex number; $\hat{d}$ describes the spin degree of freedom, which is a complex unit 3-vector satisfying $\hat{d}^*\cdot\hat{d} = 1$; $\mathrm{i}\sigma^\mu\sigma^y(\mu = x, y, z)$ form the bases of the 2×2 symmetric matrices for the triplet pairing. The so-called unitary pairing means that $\Delta^\dagger(\vec{k})\Delta(\vec{k})$ equals the identity matrix up to a constant, i.e. $\Delta(\vec{k})$ is proportional to a unitary matrix. In terms of the d-vector language, the unitary pairing corresponds to $\hat{d}^* \times \hat{d} = 0$, i.e. $\hat{d}$ is equivalent to a unit real vector up to an overall complex phase.

The two most prominent superfluid phases of ^{3}He are B and A phases, both of which belong to the class of unitary pairing. In the B phase [86], a typical pairing matrix structure is

$$\Delta^B_{\alpha\beta}(\vec{k}) = \Delta\hat{k}\cdot(\vec{\sigma}\mathrm{i}\sigma^y)_{\alpha\beta}, \tag{74}$$

where Δ is a complex constant. In this configuration, L and S are combined into $J = 0$ and thus, the B phase is rotationally invariant and also a fully gapped phase. In other words,

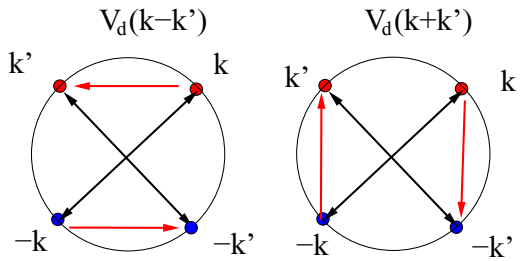

Figure 5. Pairing interaction matrix elements for the single component dipolar interaction $V_t(\vec{k};\vec{k}') = V_d(\vec{k}-\vec{k}') - V_d(\vec{k}+\vec{k}')$ due to the two-particle interference and the Fermi statistics.

the B phase spontaneously breaks the relative SO symmetry, exhibiting the SO coupled paired structure. It maintains TR and parity symmetries. Furthermore, it has also been recently found that the B phase is actually a 3D topological superfluid phase. In comparison, the ^{3}He-A phase is anisotropic, in which L and S are decoupled and J is not well-defined [87, 88]. A typical pairing matrix for the A phase is

$$\Delta^A_{\alpha\beta}(\vec{k}) = \Delta(\hat{k}_x + \mathrm{i}\hat{k}_y)(\hat{d}\cdot\vec{\sigma}\mathrm{i}\sigma^y)_{\alpha\beta}, \tag{75}$$

in which $\hat{d}$ is an arbitrary unit 3-vector. It breaks TR symmetry and exhibits nodal points on the north and south poles on the Fermi surface.

We will see in this section and in section 6 that both the electric and magnetic dipolar fermion systems support novel p-wave triplet structures which are different from the ^{3}He-B and A phases.

5.2. The p_z-wave pairing with the single-component dipolar fermions

The pairing symmetry structure of the single-component dipolar system was studied in early works of [28, 29]. In this case, the gap function is simplified as a complex number and thus, the d-vector notation is not needed.

In real space, this p_z-pairing symmetry is also clear since the electric dipolar interaction is the most attractive if the displacement vector between two fermions is along the z-axis. Below, we present the partial wave analysis in momentum space. The pairing interaction can be expressed at the mean-field level as [28, 29]

$$\begin{aligned} H_{\mathrm{pair}} &= \frac{1}{2V_0}\sum_{k,k'} V_d(\vec{k}-\vec{k}')\psi^\dagger(\vec{k})\psi^\dagger(-\vec{k})\psi(-\vec{k}')\psi(\vec{k}'), \\ &= \frac{1}{4V_0}\sum_{k,k'} V_t(\vec{k};\vec{k}')\psi^\dagger(\vec{k})\psi^\dagger(-\vec{k})\psi(-\vec{k}')\psi(\vec{k}'), \end{aligned} \tag{76}$$

where

$$V_t(\vec{k};\vec{k}') = V_d(\vec{k}-\vec{k}') - V_d(\vec{k}+\vec{k}') \tag{77}$$

satisfying $V_t(\vec{k};\vec{k}') = V_t(-\vec{k};\vec{k}') = -V_t(\vec{k},\vec{k}')$ as shown in figure 5. The symbol V_t is used because the pairing analysis here is the same as that for the triplet pairing of the two-component dipolar fermions in section 5.3.

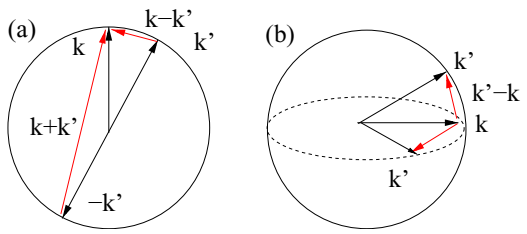

Figure 6. Pairing interaction matrix elements for the dipolar interaction $V_t(\vec{k};\vec{k}')$. (*a*) For the case of $\vec{k} \parallel \hat{z}$ and $\vec{k}' \to \vec{k}$, $V_t(\vec{k};\vec{k}') = V_t(\vec{k};-\vec{k}') < 0$. (*b*) For the case of $\vec{k} \parallel \hat{x}$ and $\vec{k}' \to \vec{k}$, $V_t(\vec{k};\vec{k}')$ varies and its angular average is positive.

The BCS mean-field gap equation is

$$\Delta(\vec{k}) = -\int \frac{\mathrm{d}^3k'}{(2\pi)^3} V_t(\vec{k};\vec{k}')[K(\vec{k}') - \frac{1}{2\epsilon_k}]\Delta(\vec{k}'), \tag{78}$$

where $E(\vec{k}) = \sqrt{(\epsilon_k-\mu)^2+\Delta^2(\vec{k})}$ and $K(\vec{k}) = \tanh[\frac{\beta}{2}E(\vec{k})]/[2E(\vec{k})]$. The integral of equation (78) has been regularized following the t-matrix method at the level of the Born approximation. This regularization is equivalent to truncate the energy away from the Fermi energy $\pm\bar{\omega}$ and $\bar{\omega}$ is at the order of the Fermi energy [29].

Although the p_z-pairing is very intuitive in the real space, it is not so obvious in momentum space. Before performing the partial-wave analysis, a qualitative momentum space picture can reveal why the p_z-pairing is natural as shown in figure 6(*a*). Let us set $\vec{k} \parallel \hat{z}$ and $\vec{k}' \to \vec{k}$, then $(\vec{k}-\vec{k}') \perp \hat{z}$ and $(\vec{k}+\vec{k}') \parallel \hat{z}$, thus

$$V_t(\vec{k};\vec{k}') = -4\pi d^2 < 0, \quad V_t(\vec{k};-\vec{k}') = 4\pi d^2 > 0, \tag{79}$$

which favors the pairing in polar regions with an odd parity. On the other hand, if we set $\vec{k}$ in the equatorial plane, say, $\vec{k} \parallel \hat{x}$ and also $\vec{k}' \to \vec{k}$, then $\vec{k}-\vec{k}'$ lies in the yz-plane. The value of $V_d(\vec{k}-\vec{k}')$ depends on the polar angle of the vector of $\vec{k}-\vec{k}'$. Its average is $\frac{2\pi}{3}d^2$ and that of $V_d(\vec{k}+\vec{k}') = -\frac{4\pi}{3}d^2$, thus the average of $V_t(\vec{k};\vec{k}')$ as $\vec{k}' \to \vec{k}$ for $\vec{k}$ in the equatorial plane is positive. This means that the pairing amplitude is suppressed in the equatorial plane. Combining the pairing structures both in the polar region and the equatorial plane, it is clear that the pairing symmetry is mostly of the p_z-wave, which is also consistent with the real space picture of pairing.

Around T_c, the gap equation can be linearized. The standard pairing eigenvalue analysis is performed by defining the eigenvectors $\phi^i_{t,s}(\hat{k})$ satisfying the eigen-equation

$$N_0 \int \mathrm{d}\Omega_{k'} V_t(\hat{k};\hat{k}')\phi^i_t(\hat{k}') = w^i_t \phi^i_{t,s}(\hat{k}), \tag{80}$$

where w^i_t are eigenvalues; N_0 is the density of states on the Fermi surface; i is the index of eigenvectors. The actual pairing occurs in the channel with the lowest negative eigenvalue. The spherical harmonics decomposition of $V_{t,s}(\vec{k};\vec{k}')$ reads

$$\frac{N_0}{4\pi} V_t(\vec{k};\vec{k}') = \sum_{l,l';m} V_{ll';m} Y^*_{lm}(\Omega_k) Y_{l'm}(\Omega_{\vec{k}'}), \tag{81}$$

where l and l' only take odd values. Compared with equations (19) and (20), we arrive at

$$V_{ll';m} = -\frac{2N_0 f_{ll';m}}{\sqrt{(2l+1)(2l'+1)}}. \tag{82}$$

The diagonalization shows that the most negative eigenvalue lies in the sector with $m = 0$, whose eigenvalue and eigenvector are

$$w^{i=0}_{t,m=0} = -3.82\lambda, \quad \phi^z(\Omega_k) \approx 0.99Y_{10} - 0.12Y_{30}. \tag{83}$$

The above pairing eigenvector shows that the pairing symmetry is mainly of the p_z-type, in agreement with the intuitive real space analysis. The pairing eigen-values in the sector of $m = 0$ can even been solved analytically as shown in [29] as $w^i_{t,m=0} = -12\lambda/[\pi(2i+1)^2]$. The gap function of equation (83) vanishes for quasi-particle momenta lying in the equatorial plane and thus exhibits a nodal plane in the Bogoliubov excitation spectra.

As shown in [29], the standard mean-field value of T_c is related to the eigenvalue solved above as

$$T_c = \frac{2e^{\gamma}\bar{\omega}}{\pi} e^{\frac{1}{w^0_t}}, \tag{84}$$

where $\gamma = 0.5772$ is the Euler constant. In [29], a further analysis based on Gor'kov, Melik–Barkhudarov (GM) approach [95] is performed, which takes into account the media polarization effect due to the virtual process of creating particle-hole excitations. This GM approach shows that the energy cutoff effect can be approximated by $\bar{\omega} \approx 0.42\epsilon_f$.

5.3. Competition between the triplet and singlet pairings in the two-component dipolar Fermi gases

The new ingredient of the two-component dipolar fermions is that both the spin singlet and triplet pairings are allowed [50–53]. We define the pairing operators in these two sectors as

$$P_s(\vec{k}) = \frac{1}{\sqrt{2}}\mathrm{tr}\Big[P(\vec{k})(-\mathrm{i}\sigma^y)\Big],$$
$$P^{\mu}_t(\vec{k}) = \frac{1}{\sqrt{2}}\mathrm{tr}\Big[P(\vec{k})(-\mathrm{i}\sigma^y\sigma^{\mu})\Big], \tag{85}$$

with $\mu = x, y, z$, respectively, where $P_{\alpha\beta}(\vec{k}) = \psi_\alpha(\vec{k})\psi_\beta(-\vec{k})$. Then the pairing Hamiltonian is expressed as

$$H_{\mathrm{pair}} = \frac{1}{2V_0}\sum_{k,k'}\Big\{ V_t(\vec{k};\vec{k}')\Big[\sum_{\mu=x,y,z} P^{\dagger,\mu}_t(\vec{k})P^{\mu}_t(\vec{k}')\Big] + V_s(\vec{k};\vec{k}')P^{\dagger}_s(\vec{k})P_s(\vec{k}')\Big\}, \tag{86}$$

where $V_{t,s}(\vec{k};\vec{k}') = V_d(\vec{k}-\vec{k}') \mp V_d(\vec{k}+\vec{k}')$ are pairing interactions in the singlet and triplet channels, respectively. The Bogoliubov quasiparticle spectra become $E_i(\vec{k}) = \sqrt{(\epsilon_k-\mu)^2+\lambda^2_i(\vec{k})}$ and $\lambda^2_{1,2}(\vec{k})$ are the eigenvalues of the positive-definite Hermitian matrix $\Delta^{\dagger}(\vec{k})\Delta(\vec{k})$.

The gap equation takes the matrix form as

$$\Delta_{\alpha\beta}(\vec{k}) = -\int \frac{\mathrm{d}^3k'}{(2\pi)^3} V_d(\vec{k}-\vec{k}')\langle|\psi_\alpha(\vec{k})\psi_\beta(-\vec{k})|\rangle, \tag{87}$$

where $\langle||\rangle$ means the thermal ensemble average. $\Delta_{\alpha\beta}(\vec{k})$ can be decomposed into the singlet and triplet channel pairings as

$$\Delta_{\alpha\beta}(\vec{k}) = \Delta_s(\vec{k})\mathrm{i}\sigma^y_{\alpha\beta} + \Delta_{t,\mu}(\vec{k})(\mathrm{i}\sigma^\mu\sigma^y)_{\alpha\beta}, \tag{88}$$

in which Δ_s and $\Delta_{t,\mu}$ satisfy

$$\Delta_{t(s),\mu}(\vec{k}) = -\frac{1}{2}\sum_i \int \frac{\mathrm{d}^3k'}{(2\pi)^3} V_{t(s)}(\vec{k};\vec{k}')[K_i(\vec{k}') - \frac{1}{2\epsilon_k}]\Delta_{t(s),\mu}(\vec{k}'), \tag{89}$$

where $K_i(\vec{k}) = \tanh[\frac{\beta}{2}E_i(\vec{k})]/[2E_i(\vec{k})]$. After linearizing the gap equation around T_c, we perform the eigenvalue analysis for the pairing problem. The eigen-equation of the triplet sector is the same as equation (80), while that of the singlet sector can be obtained by replacing $V_t(\vec{k};\vec{k}')$ with $V_s(\vec{k};\vec{k}')$. The spherical harmonics decomposition of $V_s(\vec{k};\vec{k}')$ can be done in a similar way to equation (81) and the resultant $V_{ll';m}$ takes the same form as equation (82) but with l, l' only taking even integer values. However, the Hartree interaction does not exist in the pairing channel and thus, for $l = l' = m = 0$, $V_{00;0} = 0$ for the case of the purely dipolar interaction.

The analysis of pairing eigenvalues in the triplet sector is the same as that in the single component case. Thus, the leading pairing symmetry still lies in the p_z-channel. The pairing eigenvalue and eigenvector are the same as equation (83) and T_c is still approximately determined by equation (84). We can express the triplet pairing in terms of the d-vector as

$$\Delta_{t,\mu}(\vec{k}) = \Delta_t \mathrm{e}^{\mathrm{i}\gamma}\phi^z(\Omega_k)\hat{d}_\mu, \tag{90}$$

where γ is the U(1) phase and Δ_t is the pairing amplitude. This spin-triplet pairing breaks the U(1) gauge symmetry in the charge channel and the SU(2) symmetry in the spin channel and thus, there are two different low energy excitations: phonon and spin-wave modes. This pairing is still invariant under a combined Z_2-symmetry of $\hat{d}_\mu \to -\hat{d}_\mu$ and $\gamma \to \gamma+\pi$ [96, 97] and thus, it supports two different classes of vortices: the usual integer vortex of superfluidity and the half-integer quantum vortex of superfluidity combined with a π-disclination of the d-vector.

In the singlet channel, the lowest eigenvalue and the corresponding eigenvector are

$$w_s^0 = -1.93\lambda, \quad \psi^{s+d}(\Omega_k) \approx 0.6Y_{00} - 0.8Y_{20}, \tag{91}$$

respectively. The eigenvector mixes the s and $d_{k^2-3k_z^2}$-channels. All other negative eigenvalues are small and negligible. Although for the purely dipolar interaction, the singlet channel pairing instability is significantly weaker than that of the triplet channel. Nevertheless, the matrix element $V_{00;0}$ may receive additional contributions from the short-range s-wave scattering interaction, which in principle is tunable through Feshbach resonances. At $V_{00;0}/\lambda \approx -3.15$, the singlet and triplet channel instabilities become degenerate.

Considering the competition between the spin triplet and singlet channel pairings, we generally expect two pairing superfluid transitions. The first transition is triggered by the stronger pairing channel, say, the triplet p_z-channel, which determines T_{c1}. In the case that the singlet channel pairing is weaker but nearly degenerate with the triplet one, a second transition may occur at T_{c2} as further lowering temperature. The mixing between the single and triplet pairings breaks parity and thus, the second transition is also a genuine phase transition. The coupling between these two pairing channels can be captured by the following Ginzburg–Landau (GL) free energy as [50]

$$\Delta F = \gamma_1(\vec{\Delta}_t^* \cdot \vec{\Delta}_t)|\Delta_s|^2 + \gamma_2\{\vec{\Delta}_t^* \cdot \vec{\Delta}_t^* \Delta_s\Delta_s + \mathrm{cc}\} + \gamma_3|\vec{\Delta}_t^* \times \vec{\Delta}_t|^2, \tag{92}$$

where $\vec{\Delta}_t$ is a compact notation for $\Delta_{t,\mu}(\mu = x, y, z)$; other non-gradient terms in the GL free energy only depend on the magnitudes of order parameters. γ_3 should be positive, such that $\vec{\Delta}_t$ can be described by a real d-vector multiplied by a $U(1)$ phase. The sign of γ_2 determines the relative phase between Δ_s and $\vec{\Delta}_t$: if $\gamma_2 < 0$, the phase difference between Δ_s and $\vec{\Delta}_t$ is 0 or π; if $\gamma_2 > 0$, the phase difference is $\pm\frac{\pi}{2}$. The latter case gives rise to a novel pairing with TR symmetry breaking as explained in section 5.4.

In SO coupled systems, the coupling between the singlet and triplet pairings through a spatial gradient is considered in [98], which leads to a spatially non-uniform state. Nevertheless, because of the spin conservation, such a term is not allowed in electric dipolar systems.

5.4. TR symmetry breaking mixing between the singlet and triplet pairings

When the singlet and triplet channel pairings coexist, a natural question is: what is the relative phase between these two pairing channels? It was found in [50] that, at the mean-field level, the phase difference of $\pm\frac{\pi}{2}$ between Δ^s and $\Delta^{t,\mu}$ is favored, so that TR symmetry is spontaneously broken. This is a general mechanism leading to the TR symmetry breaking pairing, which applies for the mixing problem between singlet and triplet pairings in the absence of SO coupling in the weak coupling limit. It has also been found later in [52, 53] that the TR symmetry breaking also exists in the resonance interaction regime of the dipolar Fermi gases.

The reason for the above TR symmetry breaking effect is that the weak coupling theory favors the unitary pairing, i.e. $\Delta^\dagger(\vec{k})\Delta(\vec{k})$ is an identity matrix up to a factor. A simple calculation shows that $\Delta^\dagger(\vec{k})\Delta(\vec{k}) = |\Delta^s|^2 + |\Delta^{t,\mu}|^2 + \mathrm{Re}(\Delta^{s,*}\Delta^{t,\mu})(\sigma^\mu)^T$. The unitary pairing is achieved if and only if a phase difference $\mathrm{e}^{\mathrm{i}\phi} = \pm i$ exists between Δ^s and $\Delta^{t,\mu}$. More precisely, it can be proved following the method presented in [99]. The quasi-particle spectra read $E_i = \sqrt{\xi^2 + \lambda_i^2}(i = 1, 2)$ with

$$\lambda_{1,2}^2 = |\Delta_s\phi^{s+d}(\Omega_k)|^2 + |\Delta_t\phi^z(\Omega_k)|^2 \pm 2\mathrm{Re}(\Delta_s^*\Delta_t)\phi^{s+d}(\Omega_k)\phi^z(\Omega_k). \tag{93}$$

The quasiparticle contribution to the free energy is $f(x) = -\frac{2}{\beta}\ln[2\cosh\frac{\beta}{2}\sqrt{\xi_k^2 + x}]$, which satisfies $\frac{d^2}{dx^2}f(x) > 0$ [99].

Thus,

$$f(\lambda_1^2) + f(\lambda_2^2) \geqslant 2f\left(\frac{\lambda_1^2 + \lambda_2^2}{2}\right) \tag{94}$$

and the minimum is reached at $\lambda_1^2 = \lambda_2^2$. This is precisely the condition of the unitary pairing.

Here is another intuitive view to see why the phase difference $e^{i\phi} = \pm i$ is favored. Without loss of generality, let us set $\hat{d} \parallel \hat{z}$ and assume a relative phase difference ϕ. The ratio between the pairing amplitudes is

$$\frac{\langle\psi_\uparrow(\vec{k})\psi_\downarrow(-\vec{k})\rangle}{\langle\psi_\downarrow(\vec{k})\psi_\uparrow(-\vec{k})\rangle} = \frac{\Delta_s + e^{i\phi}\Delta_t}{-\Delta_s + e^{i\phi}\Delta_t}. \tag{95}$$

Only when $e^{i\phi} = \pm i$, the magnitude of this ratio is 1, such that the pairing strengths are the same. Otherwise, say, if $e^{i\phi} = \pm 1$, the pairing amplitudes of $\langle\psi_\uparrow(\vec{k})\psi_\downarrow(-\vec{k})\rangle$ and $\langle\psi_\downarrow(\vec{k})\psi_\uparrow(-\vec{k})\rangle$ are not equal. Again, the pairing structure, whose gap magnitudes distribute over the Fermi surface in a more uniform way, is usually favored.

6. The *J*-triplet Cooper pairing with the magnetic dipolar interaction

The magnetic dipolar interaction also gives rise to novel Cooper pairing structures possessing the SO coupled nature [60]. Again, below, we use the simplest case of $F = \frac{1}{2}$ as a prototype model to explore the exotic pairing structure of the magnetic dipolar interaction, which provides a novel and robust mechanism for the p-wave ($L = 1$) spin triplet ($S = 1$) Cooper pairing. It turns out that its pairing symmetry structure is markedly different from those in the celebrated p-wave ^{3}He A and B phases: the orbital angular momentum L and spin S of a Cooper pair are coupled into the total angular momentum $J = 1$ and thus dubbed as the J-triplet pairing. In comparison, the ^{3}He B phase is isotropic in which $J = 0$; while, the A phase is anisotropic in which J is not well-defined [56].

Even within the J-triplet sector, there are still competing instabilities regarding to different possibilities of J_z's: the helical polar state ($J_z = 0$) which maintains TR symmetry and the axial state ($J_z = \pm 1$) which breaks TR symmetry. The helical polar state exhibits a pair of nodes around which the quasi-particle wavefunction exhibits winding numbers ± 1, thus it is a gapless Dirac pairing. It is a TR invariant generalization of the ^{3}He-A phase with coupled spin and orbital degrees of freedom. This state was also proposed before, in the context of superfluid ^{3}He as an intermediate phase between the ^{3}He-B phase and the normal state [66]. In contrast, the axial pairing state exhibits a Weyl type node around which the winding number is 2 and its low energy spectrum is quadratic.

In this section, we review the SO coupled pairing structure of the magnetic dipolar fermions. An intuitive real space picture for the J-triplet pairing is presented in section 6.1. The partial-wave analysis for the pairing eigenvalues is performed in section 6.2. The structure of the nodal Bogoliubov quasi-particles is given in section 6.3.

6.1. The real space picture for the *J*-triplet pairing

We perform an intuitive real space analysis based on a simple two-body problem. It can be shown that the magnetic dipolar interaction between two spin-$\frac{1}{2}$ fermions vanishes in the total spin singlet channel and it only exists in the total spin triplet channel. Naturally, the magnetic dipolar interaction leads to the triplet pairing. Let us introduce a characteristic length scale at which the kinetic energy equals the interaction energy at $a_{dp} = mg_F^2\mu_B^2/\hbar^2$ where m is the fermion mass. Since our purpose is to seek the most attractive angular partial-wave channel, without loss of generality, we can fix the inter-particle distance at a_{dp}. In the spin triplet channel, the lowest value of orbital angular momentum is p-wave and thus there are $3 \times 3 = 9$ states with $L = S = 1$. According to the total angular momentum J, they can be classified into $J = 0$, 1 and 2. The interaction energies can be easily diagonalized in each sector as

$$E_0 = E_{dp}, \quad E_1 = -\frac{1}{2}E_{dp}, \quad E_2 = \frac{1}{10}E_{dp}, \tag{96}$$

respectively, where $E_{dp} = g_F^2\mu_B^2/a_{dp}^3$. Only the channel with $J = 1$ can support bound states, which is also confirmed from the momentum space analysis below in section 6.2.

The reason why the J-triplet channel is the most attractive one is because of its particular pairing spin configuration, which shows a dominant 'head-to-tail' configuration and thus the interaction is attractive. More precisely, let us denote the spin wavefunctions and the relative orbital wavefunctions as χ_μ and $p_\mu(\hat{\Omega})$, which satisfy

$$\{\hat{e}_\mu \cdot (\vec{S}_1 + \vec{S}_2)\}\chi_\mu = 0, \quad (\hat{e}_\mu \cdot \vec{L})\, p_\mu(\hat{\Omega}) = 0, \tag{97}$$

for $\mu = x, y$ and z. In other words, χ_μ and $p_\mu(\hat{\Omega})$ are polar eigenstates of total spin and the relative orbital angular momentum, respectively. In the sector of $J = 1$, we define the SO coupled polar state satisfying

$$(\hat{e}_\mu \cdot \vec{J})\phi_\mu = 0, \tag{98}$$

which can be expressed as $\phi_\mu(\Omega) = \frac{1}{\sqrt{2}}\epsilon_{\mu\nu\lambda}\chi_\nu p_\lambda(\Omega)$. In particular, for the state with $J_z = 0$, it can be further expressed as

$$\phi_z(\hat{\Omega}) = \sqrt{\frac{3}{2}}\sin\theta\left\{|\alpha_{\hat{e}_\rho}\rangle_1|\alpha_{\hat{e}_\rho}\rangle_2 + |\beta_{\hat{e}_\rho}\rangle_1|\beta_{\hat{e}_\rho}\rangle_2\right\}, \tag{99}$$

where, $\hat{e}_\rho = \hat{x}\cos\phi + \hat{y}\sin\phi$; $|\alpha_{e_\rho}\rangle$ and $|\beta_{e_\rho}\rangle$ are eigenstates of $\hat{e}_\rho \cdot \vec{\sigma}$ with eigenvalues of ± 1, respectively. This shows the 'head-to-tail' configuration in figure 7(a) and thus, the corresponding interaction is attractive.

In contrast, the eigenstate of $J = 0$ shows the 'head-to-head' configuration as shown in figure 7(b) and thus the interaction in such a state is repulsive. It is expressed as $\phi_0(\Omega) = \frac{1}{\sqrt{2}}\left\{|\alpha_\Omega\rangle_1|\beta_\Omega\rangle_2 + |\beta_\Omega\rangle_1|\alpha_\Omega\rangle_2\right\}$, where $|\alpha_\Omega\rangle$ and $|\beta_\Omega\rangle$ are eigenstates of $\hat{\Omega} \cdot \vec{\sigma}$ with the eigenvalues ± 1, respectively.

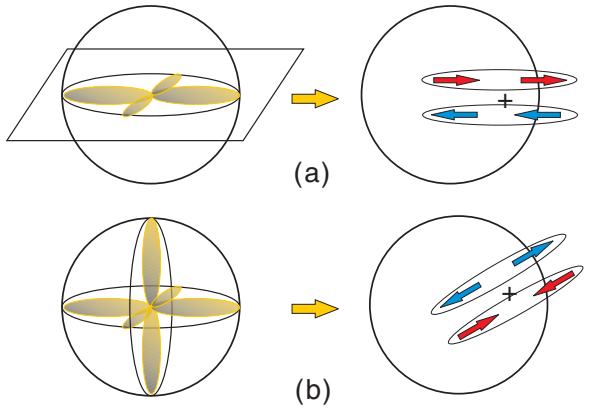

Figure 7. The spin configurations of the two-body states with (*a*) $J = 1$ and $J_z = 0$ and (*b*) $J = J_z = 0$. The average magnetic dipolar interaction is attractive in (*a*) but repulsive in (*b*). Reproduced from [60].

6.2. The momentum space partial-wave analysis

In this part, we review the partial-wave analysis in momentum space, which arrives at the same pairing symmetry as that obtained through the real space analysis.

After the mean-field decomposition, the pairing Hamiltonian of the magnetic dipolar system becomes

$$H_{mf} = \frac{1}{4}\int \frac{\mathrm{d}^3k}{(2\pi)^3}\Psi^\dagger(\vec{k})\begin{pmatrix}\xi(\vec{k})I & \Delta_{\alpha\beta}(\vec{k})\\ \Delta^*_{\beta\alpha}(\vec{k}) & -\xi(\vec{k})I\end{pmatrix}\Psi(\vec{k}), \tag{100}$$

where $\Psi(\vec{k}) = (\psi_\uparrow(\vec{k}), \psi_\downarrow(\vec{k}), \psi^\dagger_\uparrow(-\vec{k}), \psi^\dagger_\downarrow(-\vec{k}))^T$; $\xi(\vec{k}) = \epsilon(\vec{k}) - \mu$. The Bogoliubov quasiparticle spectra become $E_i(\vec{k}) = \sqrt{\xi_k^2 + \lambda_i^2(\vec{k})}$ where $i = 1, 2$ and $\lambda_i^2(\vec{k})$ are the eigenvalues of the positive-definite Hermitian matrix defined as $\Delta^\dagger(\vec{k})\Delta(\vec{k})$.

The pairing matrix $\Delta_{\alpha\beta}$ is defined as

$$\Delta_{\alpha\beta} = \sum_{S_z}\left\langle 1S_z|\frac{1}{2}\alpha\frac{1}{2}\beta\right\rangle^* \Delta_{S_z}, \tag{101}$$

where $\langle 1S_z|\frac{1}{2}\alpha\frac{1}{2}\beta\rangle$ is the Clebsch–Gordan coefficient for two spin-$\frac{1}{2}$ states to form the spin triplet. Δ_{S_z} satisfies the mean-field gap function as

$$\Delta_{S_z}(\vec{k}) = -\frac{1}{2}\sum_i \int \frac{\mathrm{d}^3k'}{(2\pi)^3} V_{S_zS'_z}(\vec{k};\vec{k}')\left[K_i(\vec{k}') - \frac{1}{2\epsilon_k}\right] \times \Delta_{S'_z}(\vec{k}'), \tag{102}$$

where $K_i(\vec{k}') = \tanh[\frac{\beta}{2}E_i(\vec{k}')]/[2E_i(\vec{k}')]$ and the integral in equation (102) is already normalized following the standard procedure [29].

The interaction matrix element in equation (102) is defined as

$$V_{S_zS'_z}(\vec{k};\vec{k}') = \frac{1}{2}\sum_{\alpha\beta\beta'\alpha'}\left\langle 1S_z|\frac{1}{2}\alpha\frac{1}{2}\beta\right\rangle\left\langle 1S'_z|\frac{1}{2}\alpha'\frac{1}{2}\beta'\right\rangle^* \times \left\{V_{\alpha\beta,\beta'\alpha'}(\vec{k}-\vec{k}') - V_{\alpha\beta,\beta'\alpha'}(\vec{k}+\vec{k}')\right\}.$$

The spherical harmonics decomposition of $V_{S_zS'_z}(\vec{k};\vec{k}')$ can be formulated as

$$\frac{N_0}{4\pi}V_{S_zS'_z}(\vec{k};\vec{k}') = \sum_{LM,L'M'} V_{LMS_z;L'M'S'_z}Y^*_{LM}(\Omega_k) \times Y_{L'M'}(\Omega_{\vec{k}'}), \tag{103}$$

where $L = L'$, or, $L = L' \pm 2$ and L, L' are odd integers. The expressions of the dimensionless matrix elements $V_{LMS_z;L'M'S'_z}$ are the same as those in equation (56) except an overall minus sign and a numeric factor.

The free energy can be calculated as

$$F = -\frac{2}{\beta}\sum_{i=1,2}\int \frac{\mathrm{d}^3k}{(2\pi)^3}\ln\left[2\cosh\frac{\beta E_{\vec{k},i}}{2}\right] - \frac{1}{2}\sum_{S_z,S'_z}\int\int \frac{\mathrm{d}^3k}{(2\pi)^3}\frac{\mathrm{d}^3k'}{(2\pi)^3}\left\{\Delta^*_{S_z}(\vec{k})V^{-1}_{S_zS'_z}(\vec{k};\vec{k}') \times \Delta_{S'_z}(\vec{k})\right\}, \tag{104}$$

where $V^{-1}_{S_zS'_z}(\vec{k};\vec{k}')$ is the inverse of the interaction matrix defined as

$$\sum_{S'_z}\int \frac{\mathrm{d}^3k'}{(2\pi)^3}V_{S_z,S'_z}(\vec{k};\vec{k}')V^{-1}_{S'_z,S''_z}(\vec{k}';\vec{k}'') = \delta_{\vec{k},\vec{k}''}\delta_{S_z,S''_z}.$$

In order to analyze the pairing eigenvalues, the gap equation is linearized around T_c for states around the Fermi surface. The total angular momentum quantum number J is employed to classify the eigen-gap functions denoted as $\phi^{a,JJ_z}_{S_z}(\vec{k})$, in which the index a is used to distinguish different channels with the same value of J. The eigen-equation for $\phi^{a,JJ_z}_{S_z}(\vec{k})$ is

$$N_0\int \frac{\mathrm{d}\Omega_{k'}}{4\pi}V_{S_zS'_z}(\vec{k};\vec{k}')\phi^{a;JJ_z}_{S'_z}(\vec{k}') = w^a_J\phi^{a;JJ_z}_{S_z}(\vec{k}), \tag{105}$$

where w^a_J are dimensionless eigenvalues; $\vec{k}, \vec{k}'$ are at the Fermi surface. Employing the spherical harmonics decomposition of equation (103), the most negative eigenvalue is calculated lying the channel of $J = L = 1$ as $w^{J=1} = -2\pi\lambda_m$. All other negative eigenvalues are significantly smaller. Thus, the dominant pairing channel remains in the J-triplet channel in the weak coupling theory in agreement with the real space analysis.

For later convenience, the pairing matrix in the $J = 1$ sector is represented as

$$\Delta^\mu_{\alpha\beta}(\vec{k}) = \frac{\Delta}{2}\epsilon_{\mu\nu\lambda}(k_\nu\sigma_\lambda - k_\lambda\sigma_\nu)_{\alpha\beta}, \tag{106}$$

for $\mu = x, y$ and z. It represents a pairing symmetry whose angular momentum projection along the direction of $\hat{e}_\mu$ is zero, i.e. it is an eigenstate of $\hat{e}_\mu \cdot \vec{J}$ with the zero eigenvalue.

6.3. Helical polar pairing and chiral axial pairing

In the sector of $J = 1$, there are still two non-equivalent pairing possibilities: $J_z = 0$, or $J_z = \pm 1$, whose pairing matrices are $\Delta^z_{\alpha\beta}(\vec{k})$ and $\frac{1}{\sqrt{2}}\{\Delta^x_{\alpha\beta}(\vec{k}) \pm i\Delta^y_{\alpha\beta}(\vec{k})\}$, respectively. Based on the GL analysis up to the quartic order of the pairing order

parameter, it can be proved that these two are the only non-equivalent pairing symmetries under 3D rotations. Right at T_c, the Ginzburg–Landau free energy can be linearized and these two instabilities are degenerate, while this degeneracy is lifted below T_c due to the non-linearity of the Ginzburg–Landau free energy.

In quantum mechanics, if a system possesses rotation symmetry, of course, the eigenstates of its energy in the $J = 1$ sector and all of their superpositions are degenerate because of the linearity of quantum mechanics. However, the index J labeling the pairing order parameter is not the angular momentum of the many-body eigenstate. The description of a many-body system in terms of order parameters is a great simplification by only keeping a very limit but essential amount of degrees of freedom. A price to pay is that the description in terms of order parameters, say, the Landau–Ginzburg free energy, is non-linear even though quantum mechanics remains linear. This is the reason why the $J_z = 0$ and $J_z = \pm 1$ in principle are non-equivalent and the superposition law does not hold for Cooper pairing symmetries. The two pairing patterns with $J_z = 1$ and $J_z = -1$ are equivalent to each other which can be connected either by a rotation or by the TR transformation.

6.3.1. Helical polar pairing. The pairing symmetry with $J_z = 0$ is also called the J-polar pairing, characterized by the following pairing matrix $\Delta^{pl}_{\alpha\beta} = \frac{1}{2}|\Delta|[k_y\sigma_1 - k_x\sigma_2)i\sigma_2]_{\alpha\beta}$ as

$$\Delta^{pl}_{\alpha\beta} = \frac{|\Delta|}{2}\begin{bmatrix} \hat{k}_x - i\hat{k}_y & 0 \\ 0 & \hat{k}_x + i\hat{k}_y \end{bmatrix}, \qquad (107)$$

which is a unitary pairing and preserves TR symmetry. The spin-up fermions are paired in the $p_x - ip_y$ symmetry, while, the spin-down fermions are paired with the $p_x + ip_y$ symmetry. Thus, it is equivalent to a helical version of the ^{3}He-A phase. In the ^{3}He-A phase, the pairing symmetry defines an orbital angular momentum direction represented by the l-vector. Here, the z-axis plays a similar role, but due to the TR symmetry, it represents the bi-direction of the polar axis and thus it is no long a vector but a director. Thus if we rotation the polar pairing around any axis in the xy-plane for 180°, then the system returns to itself up to a global phase difference.

The Bogoliubov quasiparticle spectra are degenerate for two different spin configurations as $E^{pl}_{k,\alpha} = \sqrt{\xi_k^2 + |\Delta^{pl}(\vec{k})|^2}$ with the anisotropic gap function $|\Delta^{pl}(\vec{k})|^2 = \frac{1}{4}|\Delta|^2 \sin^2\theta_k$ depicted in figure 8. The effective linearized Hamiltonian around the north and south poles can be combined as

$$H_{\uparrow\uparrow} = \psi^\dagger(\vec{k})\begin{pmatrix} v_f(k_z - k_f) & k_x - ik_y \\ k_x + ik_y & -v_f(k_z - k_f) \end{pmatrix}\psi(\vec{k}), \qquad (108)$$

where $\psi^T(\vec{k}) = (\psi_\uparrow(\vec{k}), \psi^\dagger_\uparrow(-\vec{k}))$. equation (108) describes a Weyl fermion with a unit winding number. Combining the effective Hamiltonian for the spin down sector which is also a Weyl fermion but with an opposite chirality, the low energy Bogoliubov spectrum is 3D gapless Dirac like. If the quantization axis for the polar pairing is rotated away from the z-axis, then the spin quantization axis for the Bogoliubov quasiparticles should also be transformed accordingly.

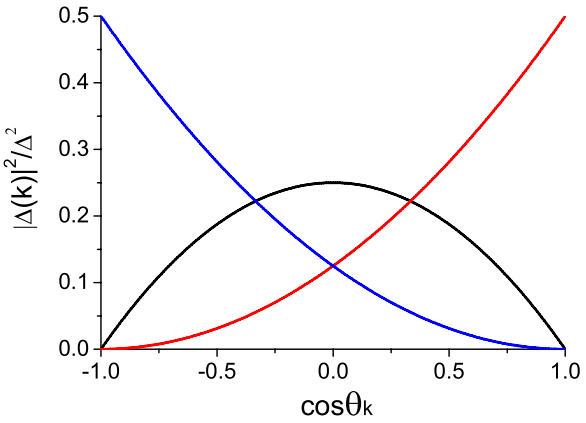

Figure 8. The angular distribution of the gap function $|\Delta(\vec{k})|^2$ versus $\cos\theta_k$ in the helical polar pairing state (the red line) and the axial pairing state (the black lines). Reproduced from [60].

6.3.2. The chiral axial pairing. Without loss of generality, we pick up the $J_z = 1$ pairing and the result of the state of $J_z = -1$ can be obtained by performing TR transformation. The pairing matrix, $\Delta^{ax}_{\alpha\beta} = \frac{1}{2\sqrt{2}}|\Delta|\{\hat{k}_z(\sigma_1 + i\sigma_2)i\sigma_2 + i\sigma_3\sigma_2(\hat{k}_x + i\hat{k}_y)\}_{\alpha\beta}$, takes the form of

$$\Delta^{ax}_{\alpha\beta}(\vec{k}) = \frac{\sqrt{2}}{2}|\Delta|\begin{bmatrix} \hat{k}_z & \frac{1}{2}(\hat{k}_x + i\hat{k}_y) \\ \frac{1}{2}(\hat{k}_x + i\hat{k}_y) & 0 \end{bmatrix}, \qquad (109)$$

thus, this is a non-unitary pairing state. The Bogoliubov quasiparticle spectra have two non-degenerate branches with anisotropic dispersion relations as $E^{ax}_i(\vec{k}) = \sqrt{\xi_k^2 + |\Delta^{ax}_i(\vec{k})|^2}$, with

$$|\Delta^{ax}_i(\vec{k})|^2 = \frac{1}{8}|\Delta|^2(1 \pm \cos\theta_k)^2 \qquad (110)$$

for $i = 1$ and 2, respectively, as depicted in figure 8.

Considering the coupling between $\vec{k}$ and $-\vec{k}$, we can combine the north and south poles together into a four component spinor. The above energy spectra show that two of them are gapped, while, another two of them are gapless forming a two-component Weyl spinor. Different from the usual linear dispersion of Weyl fermions, the dispersions are quadratic with respect to the the transverse momentum $k_\parallel = \sqrt{k_x^2 + k_y^2}$.

A natural question is: which pairing is energetically more stable? For the case of ^{3}He, at the mean-field level, the B-phase is always more stable than the A-phase [86] because the gap function of the B phase is uniform over the Fermi surface. This can be intuitively understood as follows: the BCS mean-field free energy density in momentum space $\mathcal{F}[|\Delta(\vec{k})|^2]$ can be viewed as a functional of the gap function $|\Delta(\vec{k})|^2$. Let us consider the pairing on the Fermi surface with the constraint of $\int d\Omega_k|\Delta(\vec{k})|^2$ fixed as a constant and then to minimize the free energy. Usually, the non-linearity of the free energy favors a distribution of $|\Delta_k|^2$ as uniform as possible. Here, the situation is quite subtle. As shown in figure 8, for both cases, the pairing gap function distributions on the Fermi surface are non-uniform. Nevertheless, the distribution of the unitary polar pairing is more uniform than that of the axial

pairing. Naturally, we expect that, at the mean-field level, the polar pairing wins. This has been numerically confirmed by comparing the BCS mean-field free energies of both pairings in [89]. However, we need to bear in mind that this conclusion is only valid at the mean-field level. We cannot rule out the possibility that certain strong coupling effects can stabilize the axial state. In fact, even in the ^{3}He case, the A phase wins in certain parameter regime in which the strong correlation spin feedback effect dominates [56, 88].

6.3.3. More discussions. The above study of the spin-$\frac{1}{2}$ magnetic dipolar system is just a toy model to start with. Of course, the energy scale is too small to be observed in current cold atom systems. Even for large moment atoms ^{161}Dy ($\mu = 10\mu_B$) with the current available density $10^{13}\,\mathrm{cm}^{-3}$, the dipolar energy scale is only around $6nK$ [59]. One possible way to enhance the interaction energy scale is to impose the optical lattice structure. For particles in the same lattice site, the inter-particle distance is at the order of 100 nm, which can enhance the interaction energy scale to $0.6\,\mu$K. Even the s-orbital band can hold up to $2F + 1$ fermions per site. We expect that this system can exhibit a variety of even more exotic many-body physics to be explored.

7. Conclusions

We have briefly reviewed the novel many-body physics of both electric and magnetic dipolar fermion systems focusing on the aspect of unconventional symmetries. The electric dipolar interaction is characterized by its $d_{r^2-3z^2}$-anisotropy, which leads to anisotropic Fermi liquid properties in the particle-hole channel and a robust mechanism of spin-triplet p_z-wave Cooper pairing in the particle-particle channel. The competition and coexistence between the singlet and triplet Cooper pairing leads to a novel mechanism of TR symmetry breaking pairing. The magnetic dipolar interaction manifests its SO coupled nature in unpolarized fermion systems. Its Fermi liquid theory is SO coupled whose collective zero sound mode exhibits an oscillation of a topological non-trivial spin structure over the Fermi surface. The magnetic dipolar interaction also lead to a SO coupled p-wave spin triplet Cooper pairing state with the total spin of a Cooper pair $J = 1$. This is a novel pairing symmetry different from that in both ^{3}He-B and A phases, whose Bogoliubov quasiparticles exhibit nodal helical Dirac or chiral Weyl spectra.

Acknowledgments

We thank C K Chan, S Das Sarma, J Hirsch, W C Lee and K Sun for collaborations. In particular, CW is grateful to S Das Sarma for introducing the field of dipolar fermions to him. We also thank E Fradkin, A J Leggett, S Kivelson, S C Zhang and F Zhou for helpful discussions and encouragements. C W acknowledges the support from AFOSR FA9550-14-1-0168, NSF-DMR 1410375 and the NSF of China under Grant No. 11328403. Y L thanks the support at the Princeton Center for Theoretical Science.

References

[1] Lahaye T, Menotti C, Santos L, Lewenstein M and Pfau T 2009 *Rep. Prog. Phys.* **72** 126401
[2] Lahaye T, Metz J, Fröhlich B, Koch T, Meister M, Griesmaier A, Pfau T, Saito H, Kawaguchi Y and Ueda M 2008 *Phys. Rev. Lett.* **101** 080401
[3] Menotti C, Lewenstein M, Lahaye T and Pfau T 2008 *AIP Conf. Proc.* **970** 332
[4] Menotti C and Lewenstein M 2008 *Recent Progress in Many-Body Theories* ed J Boronat *et al* (Singapore: World Scientific) pp 79–93
[5] Griesmaier A, Werner J, Hensler S, Stuhler J and Pfau T 2005 *Phys. Rev. Lett.* **94** 160401
[6] Trefzger C, Menotti C, Capogrosso-Sansone B and Lewenstein M 2011 *J. Phys. B: At. Mol. Phys.* **44** 193001
[7] Lian B, Ho T-L and Zhai H 2012 *Phys. Rev.* A **85** 051606
[8] Ni K-K, Ospelkaus S, de Miranda M H G, Pe'er A, Neyenhuis B, Zirbel J J, Kotochigova S, Julienne P S, Jin D S and Ye J 2008 *Science* **322** 231
[9] Ospelkaus S, Ni K, Wang D, de Miranda M H G, Neyenhuis B, Quéméner G, Julienne P S, Bohn J L, Jin D S and Ye J 2010 *Science* **327** 853
[10] Ni K, Ospelkaus S, Wang D, Quéméner G, Neyenhuis B, de Miranda M H G, Bohn J L, Ye J and Jin D S 2010 *Nature* **464** 1324
[11] Chotia A, Neyenhuis B, Moses S A, Yan B, Covey J P, Foss-Feig M, Rey A M, Jin D S and Ye J 2012 *Phys. Rev. Lett.* **108** 080405
[12] Wu C-H, Park J W, Ahmadi P, Will S and Zwierlein M W 2012 *Phys. Rev. Lett.* **109** 085301
[13] Yan B, Moses S A, Gadway B, Covey J P, Hazzard K R A, Rey A M, Jin D S and Ye J 2013 *Nature* **501** 521
[14] Hazzard K R A, Gadway B, Foss-Feig M, Yan B, Moses S A, Covey J P, Yao N Y, Lukin M D, Ye J, Jin D S and Rey A M 2014 arXiv:1402.2354
[15] Zhu B *et al* 2014 *Phys. Rev. Lett.* **112** 070404
[16] Syzranov S V, Wall M L, Gurarie V and Rey A M 2014 arXiv:1406.0570
[17] Wall M L, Hazzard K R A and Rey A M 2014 arXiv:1406.4758
[18] Aikawa K, Frisch A, Mark M, Baier S, Grimm R and Ferlaino F 2014 *Phys. Rev. Lett.* **112** 010404
[19] Aikawa K, Baier S, Frisch A, Mark M, Ravensbergen C and Ferlaino F 2014 *Science* **345** 1484
[20] Aikawa K, Frisch A, Mark M, Baier S, Grimm R, Bohn J L, Jin D S, Bruun G M and Ferlaino F 2014 arXiv:1405.1537
[21] Lu M, Youn S H and Lev B L 2010 *Phys. Rev. Lett.* **104** 063001
[22] Lu M, Youn S H and Lev B L 2011 *Phys. Rev.* A **83** 012510
[23] Youn S H, Lu M, Ray U and Lev B L 2010 *Phys. Rev.* A **82** 043425
[24] Burdick N Q, Baumann K, Tang Y, Lu M and Lev B L 2014 arXiv:1407.3842
[25] Baumann K, Burdick N Q, Lu M and Lev B L 2014 *Phys. Rev.* A **89** 020701
[26] Lu M, Burdick N Q and Lev B L 2012 *Phys. Rev. Lett.* **108** 215301
[27] Lu M, Youn S H and Lev B L 2011 *Phys. Rev.* A **83** 012510
[28] You L and Marinescu M 1999 *Phys. Rev.* A **60** 2324
[29] Baranov M A, Mar'enko M S, Rychkov V S and Shlyapnikov G V 2002 *Phys. Rev.* A **66** 013606
[30] Baranov M A, Dalmonte M, Pupillo G and Zoller P 2012 *Chem. Rev.* **112** 5012
[31] Miyakawa T, Sogo T and Pu H 2008 *Phys. Rev.* A **77** 061603
[32] Sogo T, He L, Miyakawa T, Yi S, Lu H and Pu H 2009 *New J. Phys.* **11** 055017
[33] Fregoso B M, Sun K, Fradkin E and Lev B L 2009 *New J. Phys.* **11** 103003
[34] Chan C-K, Wu C, Lee W-C and Das Sarma S 2010 *Phys. Rev.* A **81** 023602

[35] Sun K, Wu C and Das Sarma S 2010 *Phys. Rev.* B **82** 075105
[36] Ronen S and Bohn J L 2010 *Phys. Rev.* A **81** 033601
[37] Lin C, Zhao E and Liu W V 2010 *Phys. Rev.* B **81** 045115
[38] Liu B and Yin L 2011 *Phys. Rev.* A **84** 053603
[39] Li Q, Hwang E H and Das Sarma S 2010 *Phys. Rev.* B **82** 235126
[40] Kestner J P and Das Sarma S 2010 *Phys. Rev.* A **82** 033608
[41] Baranov M A, Fehrmann H and Lewenstein M 2008 *Phys. Rev. Lett.* **100** 200402
[42] Rodríguez-Ponte P, Grandi N and Cabra D C 2014 arXiv:1406.2618
[43] Fregoso B M and Fradkin E 2009 *Phys. Rev. Lett.* **103** 205301
[44] Baranov M A, Dobrek L and Lewenstein M 2004 *Phys. Rev. Lett.* **92** 250403
[45] Bruun G M and Taylor E 2008 *Phys. Rev. Lett.* **101** 245301
[46] Levinsen J, Cooper N R and Shlyapnikov G V 2011 *Phys. Rev.* A **84** 013603
[47] Potter A C, Berg E, Wang D-W, Halperin B I and Demler E 2010 *Phys. Rev. Lett.* **105** 220406
[48] Lutchyn R M, Rossi E and Das Sarma S 2010 *Phys. Rev.* A **82** 061604
[49] Zhao C, Jiang L, Liu X, Liu W M, Zou X and Pu H 2010 *Phys. Rev.* A **81** 063642
[50] Wu C and Hirsch J E 2010 *Phys. Rev.* B **81** 020508
[51] Shi T, Zhang J N, Sun C P and Yi S 2009 *Phys. Rev.* A **82** 033623
[52] Qi R, Shi Z-Y and Zhai H 2013 *Phys. Rev. Lett.* **110** 045302
[53] Shi T, Zou S-H, Hu H, Sun C-P and Yi S 2013 *Phys. Rev. Lett.* **110** 045301
[54] Liu B, Li X, Yin L and Liu W V 2014 arXiv:1407.2949
[55] Shi T, Zhang J-N, Sun C-P and Yi S 2010 *Phys. Rev.* A **82** 033623
[56] Leggett A J 1975 *Rev. Mod. Phys.* **47** 331
[57] Mackenzie A P and Maeno Y 2003 *Rev. Mod. Phys.* **75** 657
[58] Fujita T and Quader K F 1987 *Phys. Rev.* B **36** 5152
[59] Fregoso B M and Fradkin E 2010 *Phys. Rev.* B **81** 214443
[60] Li Y and Wu C 2012 *Sci. Rep.* **2** 392
[61] Sogo T, Urban M, Schuck P and Miyakawa T 2012 *Phys. Rev.* A **85** 031601
[62] Li Y and Wu C 2012 *Phys. Rev.* B **85** 205126
[63] Bhongale S G, Mathey L, Tsai S-W, Clark C W and Zhao E 2013 *Phys. Rev.* A **87** 043604
[64] Tohyama M 2013 *J. Phys. Soc. Japan* **82** 124004
[65] Ashrafi A, Rashba E I and Maslov D L 2013 *Phys. Rev.* B **88** 075115
[66] Fishman R S 1987 *Phys. Rev.* B **36** 79
[67] Wang B, Wang D-W and Das Sarma S 2010 *Phys. Rev.* A **82** 021602
[68] Bhongale S G, Mathey L, Tsai S-W, Clark C W and Zhao E 2012 *Phys. Rev. Lett.* **108** 145301
[69] Han L and de Melo C A R S 2010 arXiv:1006.2072
[70] Deng Y, Cheng J, Jing H, Sun C-P and Yi S 2012 *Phys. Rev. Lett.* **108** 125301
[71] Cui X, Lian B, Ho T-L, Lev B L and Zhai H 2013 *Phys. Rev.* A **88** 011601(R)
[72] Yao N Y, Laumann C R, Gorshkov A V, Bennett S D, Demler E, Zoller P and Lukin M D 2012 *Phys. Rev. Lett.* **109** 266804
[73] Yao N Y, Laumann C R, Gopalakrishnan S, Knap M, Mueller M, Demler E A and Lukin M D 2013 arXiv:1311.7151
[74] Kestner J P, Wang B, Sau J D and Das Sarma S 2011 *Phys. Rev.* B **83** 174409
[75] Baranov M 2008 *Phys. Rep.* **464** 71
[76] Yi S and Pu H 2008 arXiv:0804.0191
[77] Landau L 1957 *Sov. Phys.—JETP USSR* **3** 920
[78] Landau L 1959 *Sov. Phys.—JETP-USSR* **8** 70
[79] Negele J W and Orland H 1988 *Quantum Many-Particle Systems* (New York: Westview)
[80] Pomeranchuk I I 1959 *Sov. Phys.—JETP USSR* **8** 361
[81] Oganesyan V, Kivelson S A and Fradkin E 2001 *Phys. Rev.* B **64** 195109
[82] Garst M and Chubukov A V 2010 *Phys. Rev.* B **81** 235105
[83] Metlitski M A and Sachdev S 2010 *Phys. Rev.* B **82** 075127
[84] Wu C and Zhang S-C 2004 *Phys. Rev. Lett.* **93** 036403
[85] Wu C, Sun K, Fradkin E and Zhang S-C 2007 *Phys. Rev.* B **75** 115103
[86] Balian R and Werthamer N R 1963 *Phys. Rev.* **131** 1553
[87] Anderson P W and Morel P 1961 *Phys. Rev.* **123** 1911
[88] Brinkman W F, Serene J W and Anderson P W 1974 *Phys. Rev.* A **10** 2386
[89] Li Q, Hwang E H and Das Sarma S 2010 *Phys. Rev.* B **82** 235126
[90] Volovik G E and Volovik G 2009 *The Universe in a Helium Droplet* vol 117 (New York: Oxford University Press)
[91] Goswami P and Roy B 2014 *Phys. Rev.* B **90** 041301
[92] Hinojosa A, Fernandes R M and Chubukov A V 2014 arXiv:1405.7077
[93] Xia J *et al* 2008 *Phys. Rev. Lett.* **100** 127002
[94] Xia J, Maeno Y, Beyersdorf P T, Fejer M M and Kapitulnik A 2006 *Phys. Rev. Lett.* **97** 167002
[95] Gor'kov L and Melik-Barkhudarov 1961 *JETP* **40** 1452
[96] Zhou F 2003 *Int. J. Mod. Phys. B: Condens. Matter Phys.* **17** 2643
[97] Salomaa M M and Volovik G E 1987 *Rev. Mod. Phys.* **59** 533
[98] Samokhin K V and Mar'enko M S 2006 *Phys. Rev. Lett.* **97** 197003
[99] Cheng M, Sun K, Galitski V and Das Sarma S 2010 *Phys. Rev.* B **81** 024504